Molecular Cell, Volume *83*

Supplemental information

Single-molecule imaging reveals translation-dependent destabilization of mRNAs

Pratik Dave, Gregory Roth, Esther Griesbach, Daniel Mateju, Tobias Hochstoeger, and Jeffrey A. Chao

Figure S1

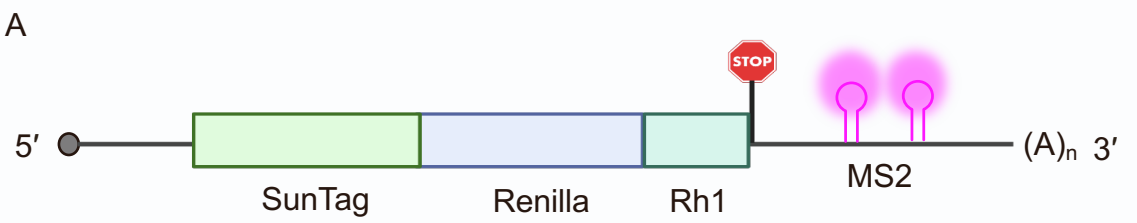

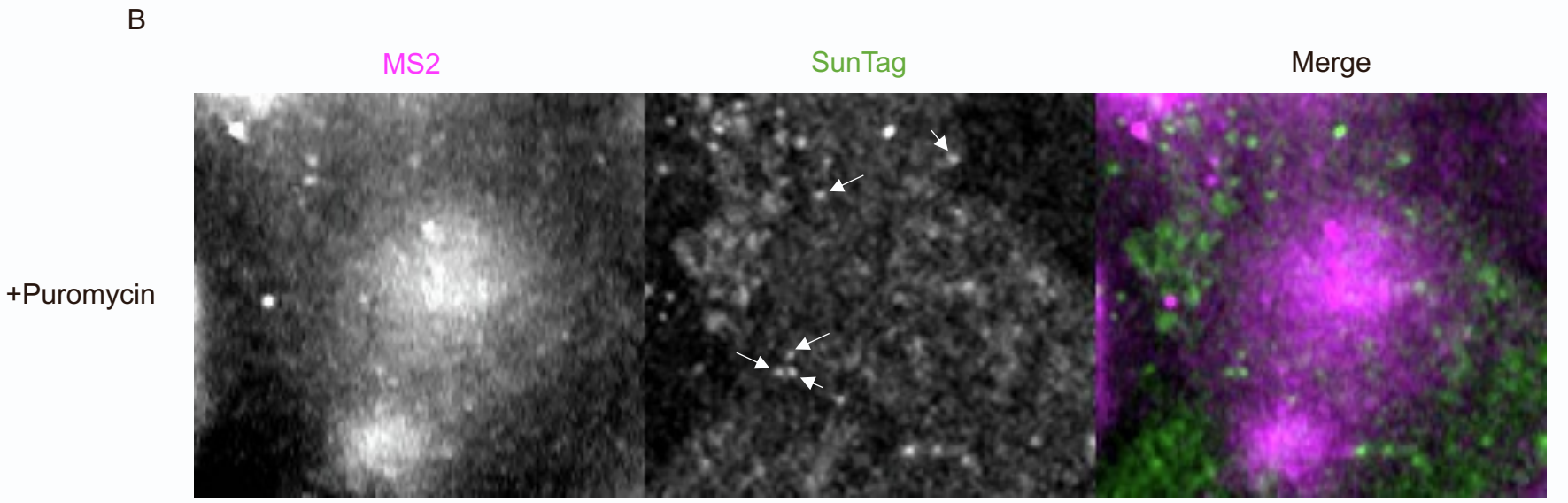

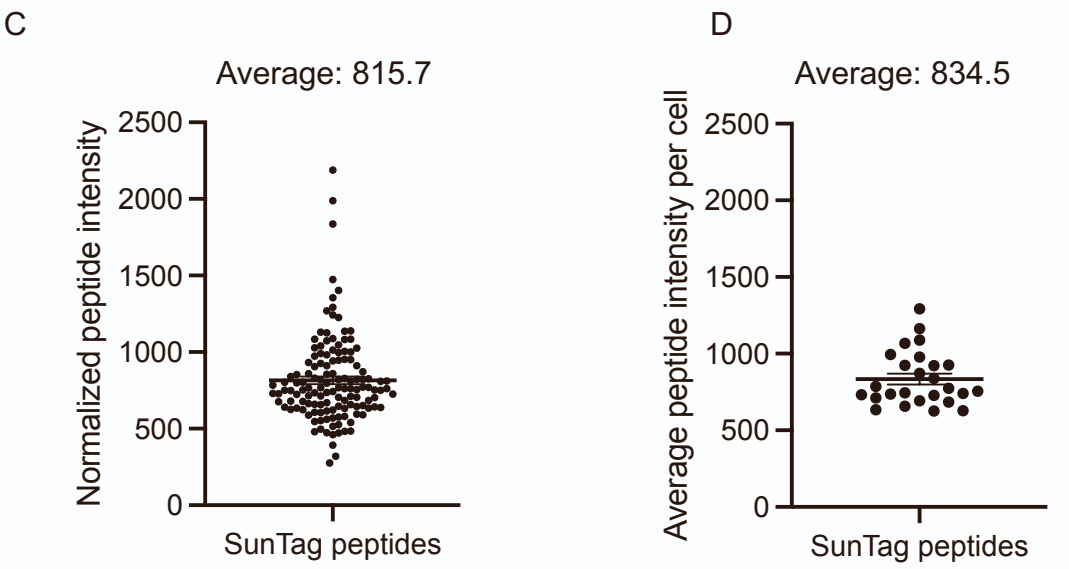

Figure S1. Quantification of intensity of single SunTag polypeptide. Related to Figure 1, Video S5

A. Schematic representation of the mRNA used to quantify the intensity of single SunTag polypeptides. Upon translation the mature SunTag polypeptide containing the Rh1 domain associates with actin-filaments allowing for stable imaging of actin-anchored individual SunTag-polypeptides.

B. Representative image of SunTag-Rh1 reporter mRNA expressed in puromycin-treated HeLa cells stably expressing MCP-Halo and scFV-GFP. Imaging was carried out after treating cells with 100 µg/mL puromycin for 10 mins to dissociate ribosomes from the mRNAs. The white arrows indicate individual SunTag-polypeptides bound to actin-filaments (See supplementary video 7).

C. Quantification of intensities of individual mature SunTag-polypeptides (background subtracted) (134 peptides, 26 cells). Mean±SEM – 815.7±24.45.

D. Average intensity of mature SunTag-peptides per cell. Mean±SEM – 834.6±34.76.

Figure S2

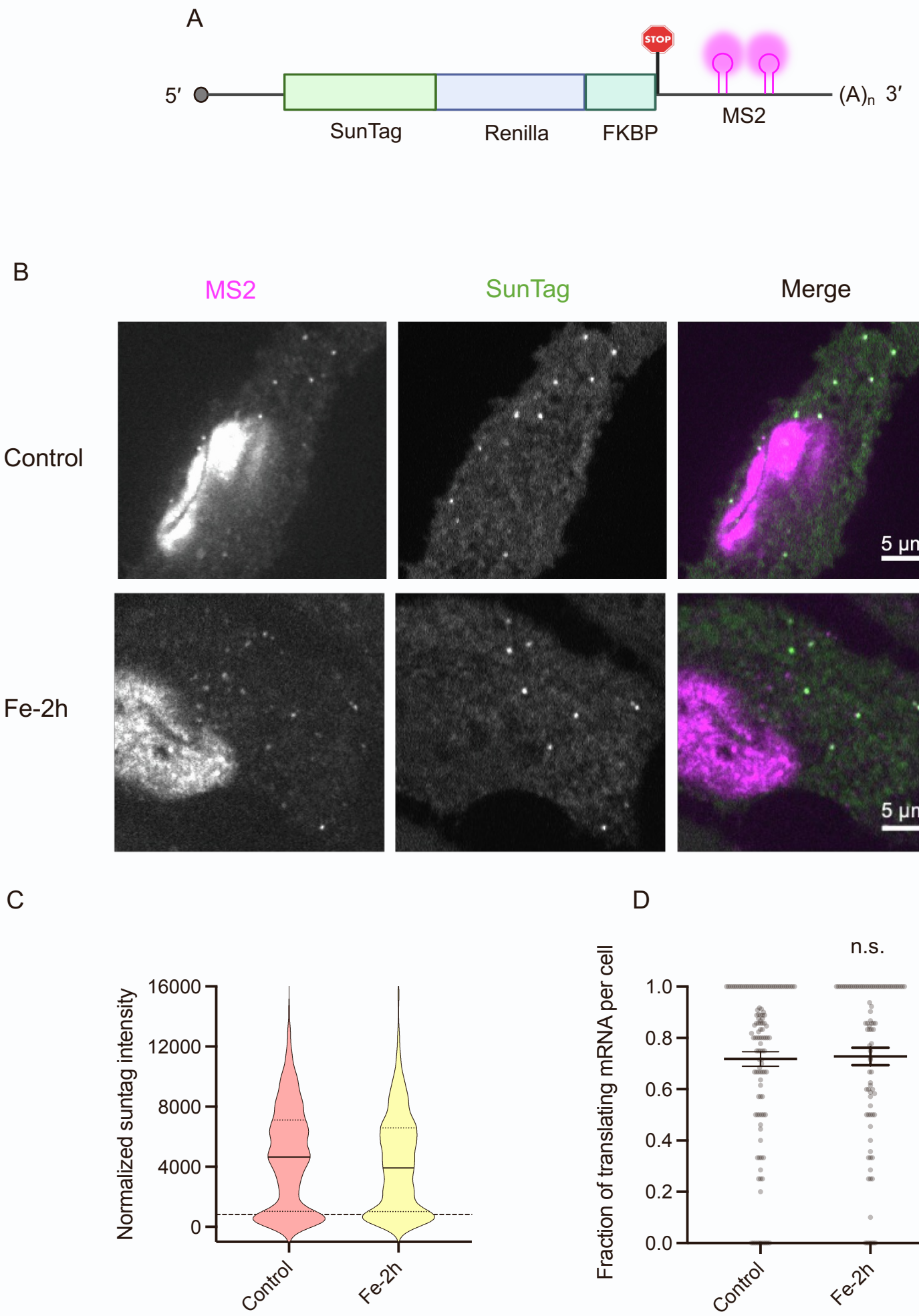

Figure S2. Iron treatment does not affect the translation of SunTag mRNAs. Related to Figure 1, Video S6, Video S7

A. Schematic representation of the SunTag mRNA used to study translation upon treatment of cells with iron.
B. Live-cell single-molecule imaging of SunTag mRNAs upon treatment of cells with iron for 2h (Fe-2h) or in absence of iron (Control). mRNAs (magenta) undergoing translation co-localize with SunTag signal (green).
C. Quantification of the background subtracted SunTag intensities in the absence of Fe (Control - 1092 mRNAs) or in the presence of iron treated for 2h (Fe-2h - 758 mRNAs), from 2 independent experiments. The dotted line represents the cut-off based on the intensity of a single SunTag polypeptide.
D. Fraction of translating mRNAs per cell in control (182 cells) and cells treated with iron for 2 hours (138 cells). Mean ± SEM is indicated, n.s. indicates not significant as compared to control.

Figure S3

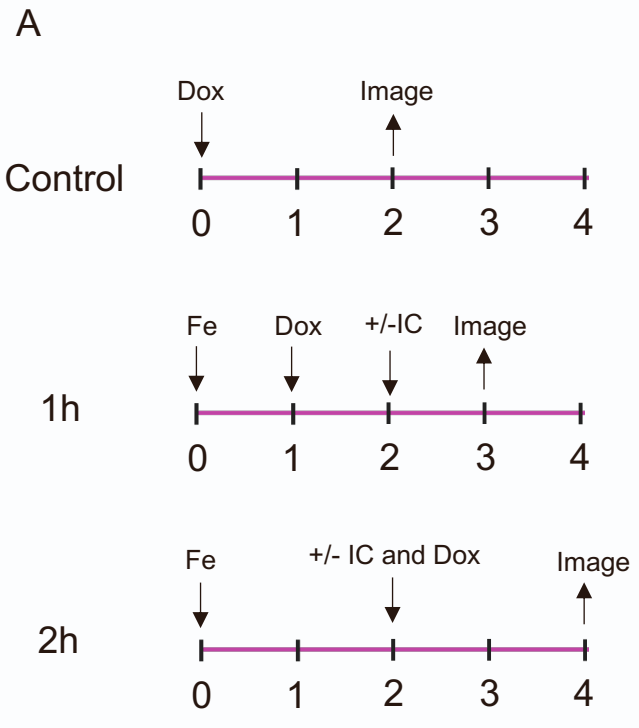

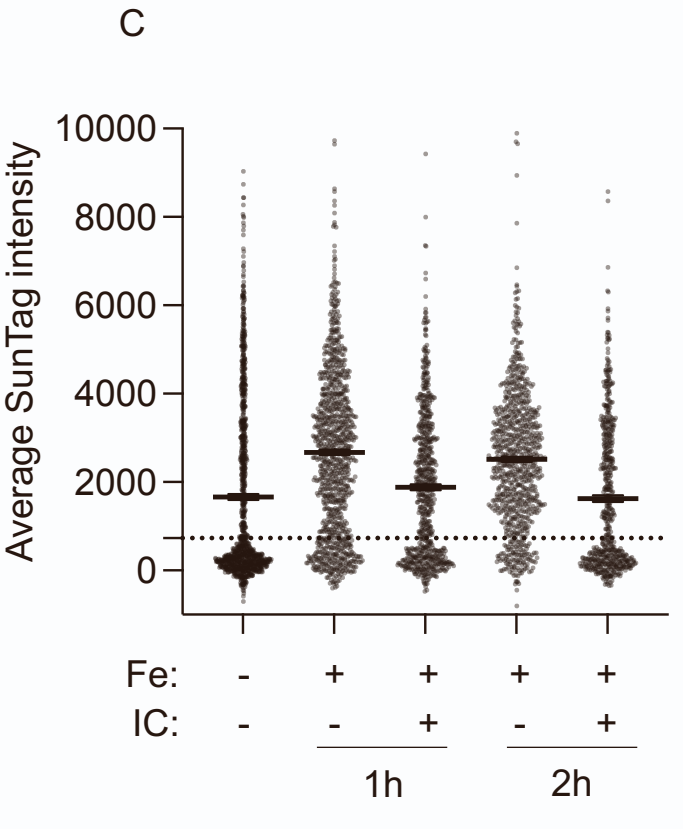

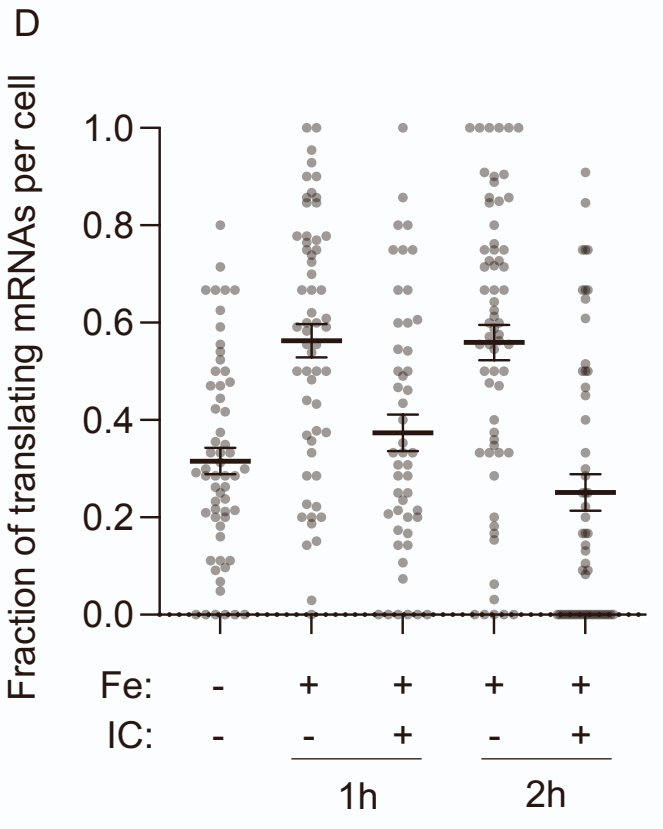

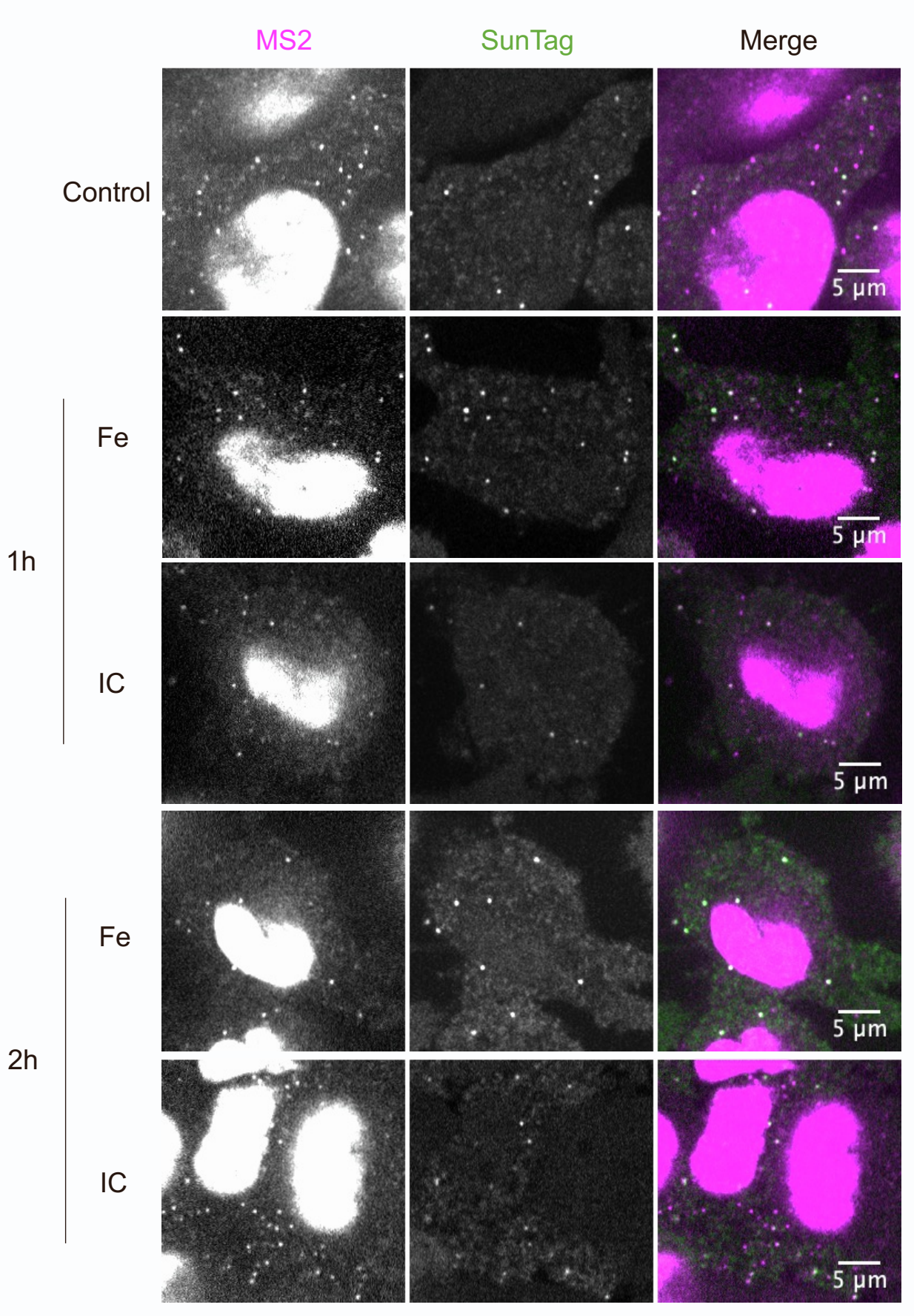

Figure S3. Reversible iron-induced translation of IRE-SunTag reporters. Related to Figure 1.

A. Schematic representation of the experiment design to study the effect of iron chelator (IC) on translation of the IRE-SunTag mRNAs. Cells were treated with iron for 2h to increase translation of the IRE-SunTag mRNAs. This was followed by treatment of cells with either 10 μM IC or DMSO for 1h or 2h hours. Untreated cells were used as control.

B. Live-cell single-molecule imaging of IRE-SunTag mRNAs in absence of iron and after treatment with 150 μM ferrous ammonium citrate as iron source for 2h (Fe-2h) or 4h (Fe-4h). mRNAs (magenta) undergoing translation co-localize with SunTag signal (green).

C. Quantification of SunTag intensities of IRE-SunTag mRNAs in the absence of iron (Control - 1078 mRNAs), in the presence of iron treated with DMSO (1h - 1050 mRNAs, 2h - 877 mRNAs), in the presence of iron treated with iron chelator (1h - 700 mRNAs, 2h - 575 mRNAs) or in the presence of iron treated for 2h (Fe-2h - 3140 mRNAs). The background GFP intensity of the cell was subtracted from the measured SunTag intensity for each mRNA. The dotted line represents the translation cutoff based on the intensity of a single SunTag polypeptide.

D. Quantification of the fraction of translating mRNAs per cell upon iron chelator treatment.

Figure S4

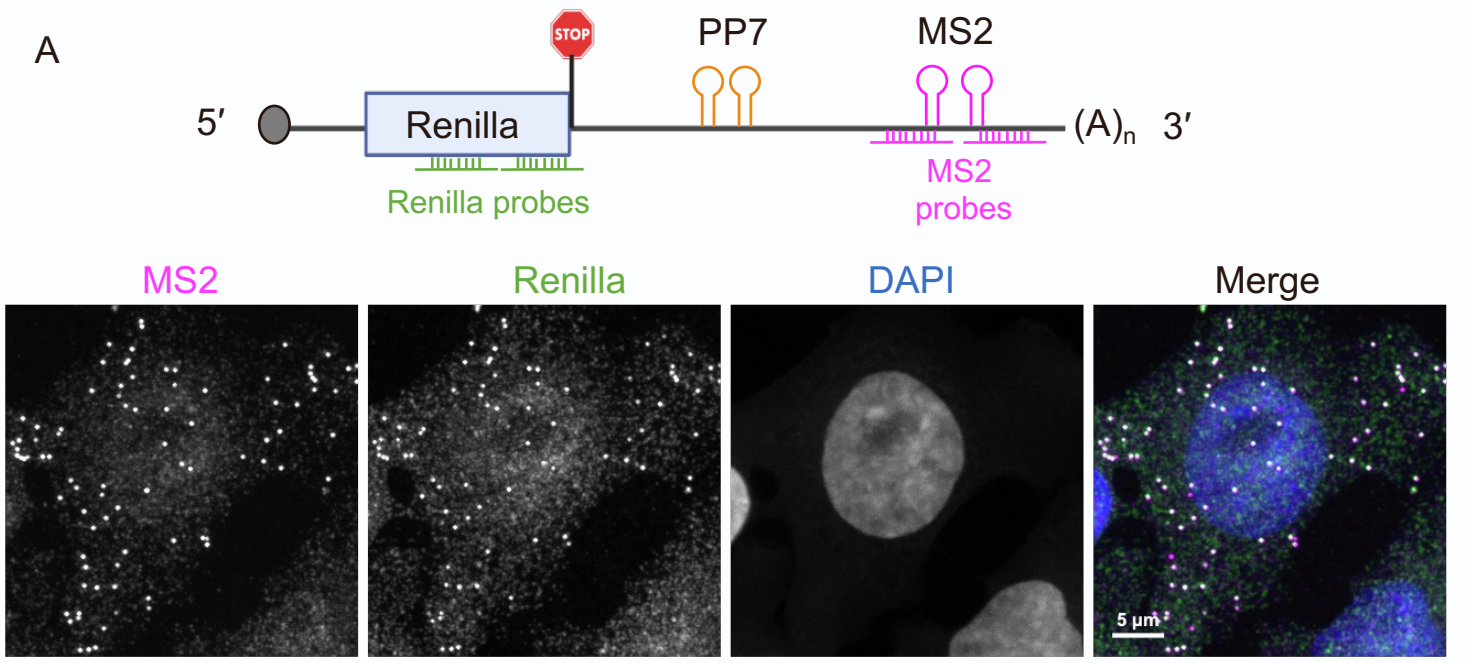

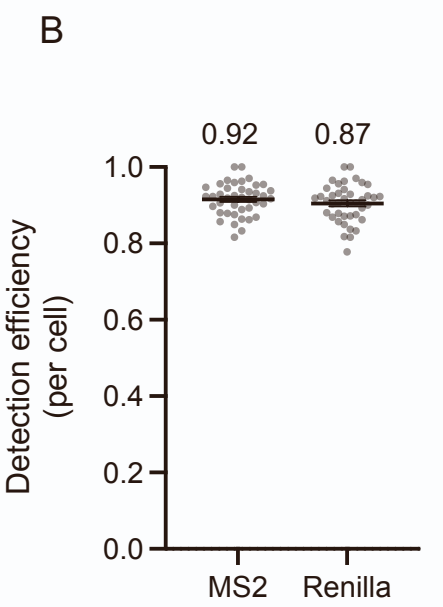

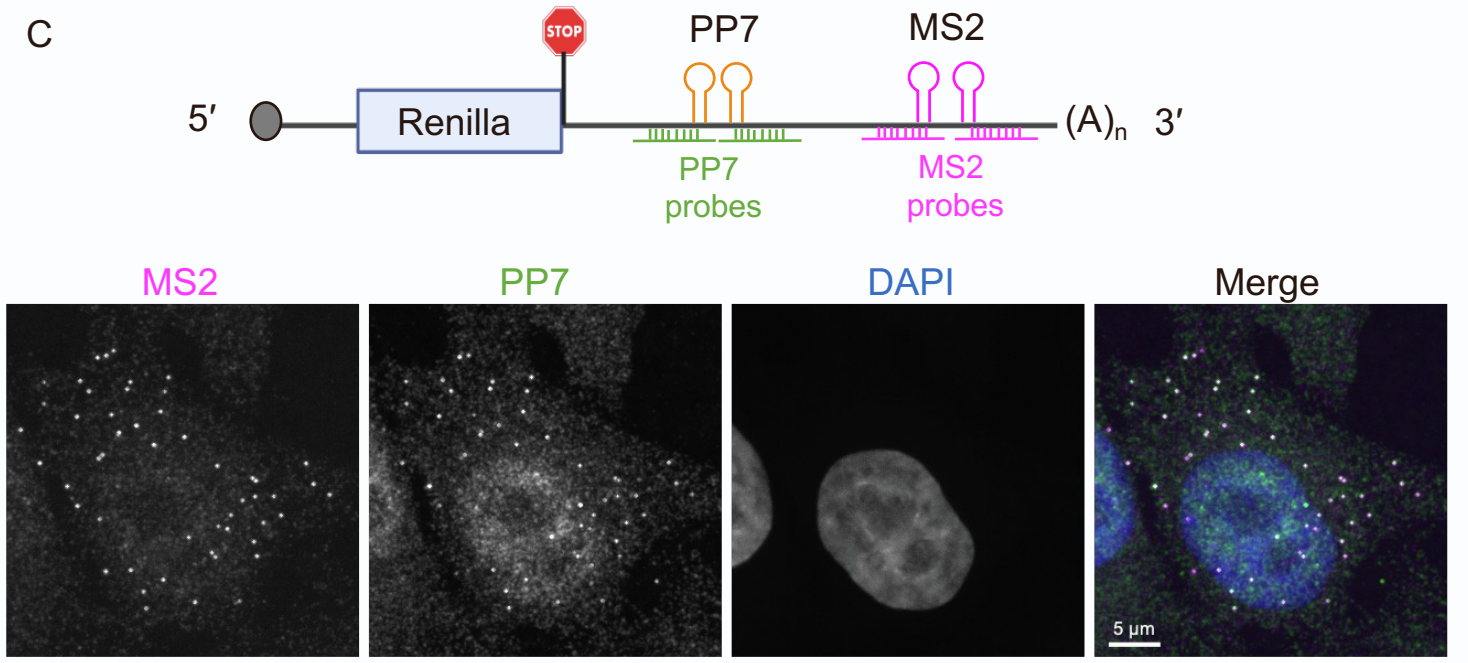

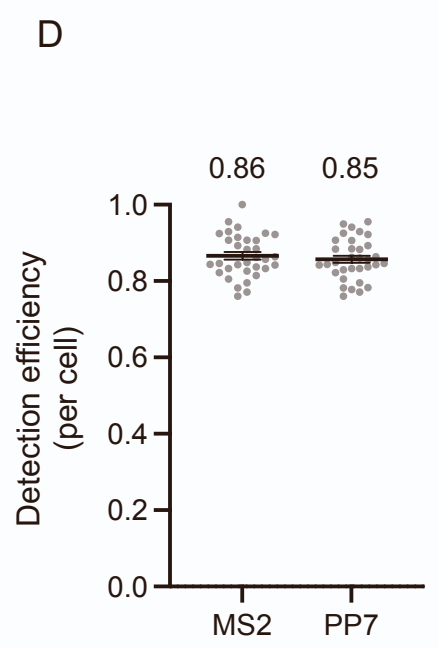

Figure S4. Determination of detection efficiencies of smFISH probes using minusPK mRNAs. Related to Figure 2.

A. Schematic representation of the -pk-TREAT mRNA, lacking the Xrn1 resistant pseudoknots, used to quantify the detection efficiency of the probes. smFISH probes (Renilla and MS2) used for studying decay kinetics in all the experiments are represented. A representative smFISH image of a cell expressing -pk-TREAT mRNAs is shown with Renilla (green) and MS2 (magenta).
B. Distribution of detection efficiency of smFISH probes (Renilla-MS2 probe pair) per cell. The mean detection efficiency of Renilla probes and MS2 probes from all the cells (41 cells) is indicated above the plot.
C. Schematic representation of the -pk-TREAT mRNA, lacking the Xrn1 resistant pseudoknots, used to quantify the detection efficiency of the probes. smFISH probes (Renilla and PP7) used for studying decay kinetics in all the experiments are represented. A representative smFISH image of a cell expressing -pk-TREAT mRNA is shown with PP7 (green) and MS2 (magenta).
D. Distribution of detection efficiency of smFISH probes (PP7-MS2 probe pair) per cell. The mean detection efficiency of PP7 probes and MS2 probes from all the cells (33 cells) is indicated above the plot.

Figure S5

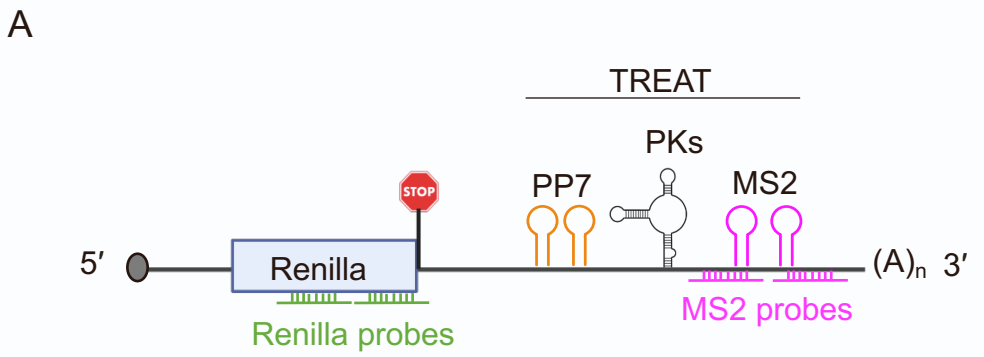

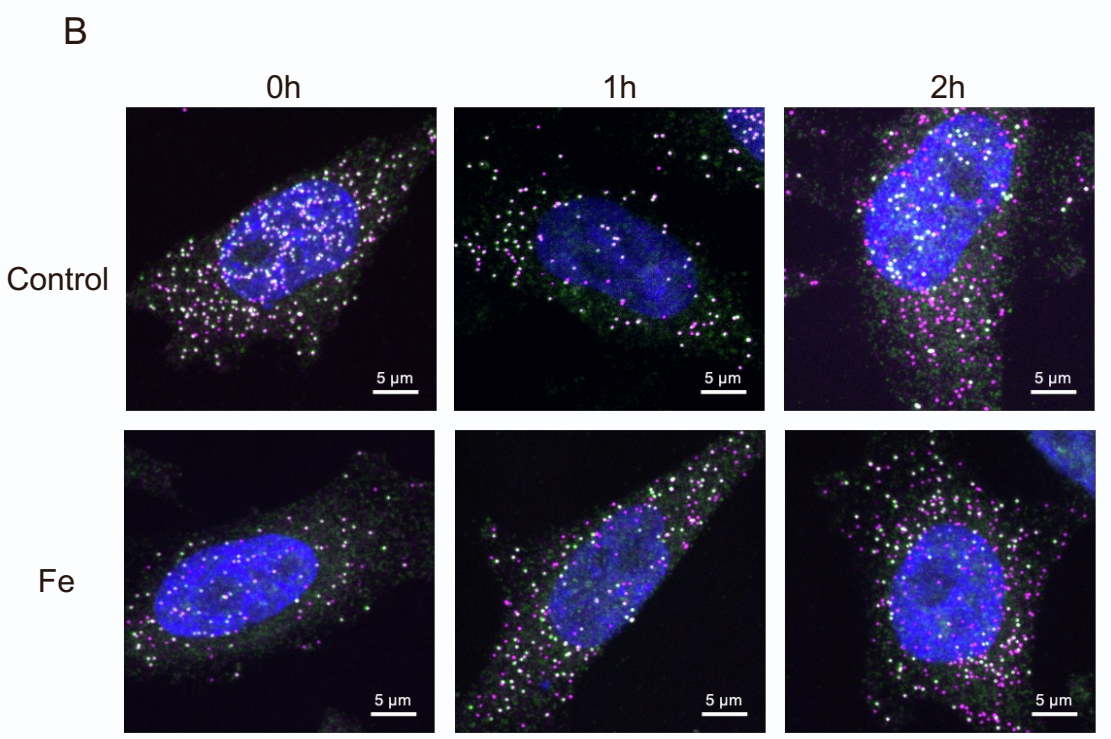

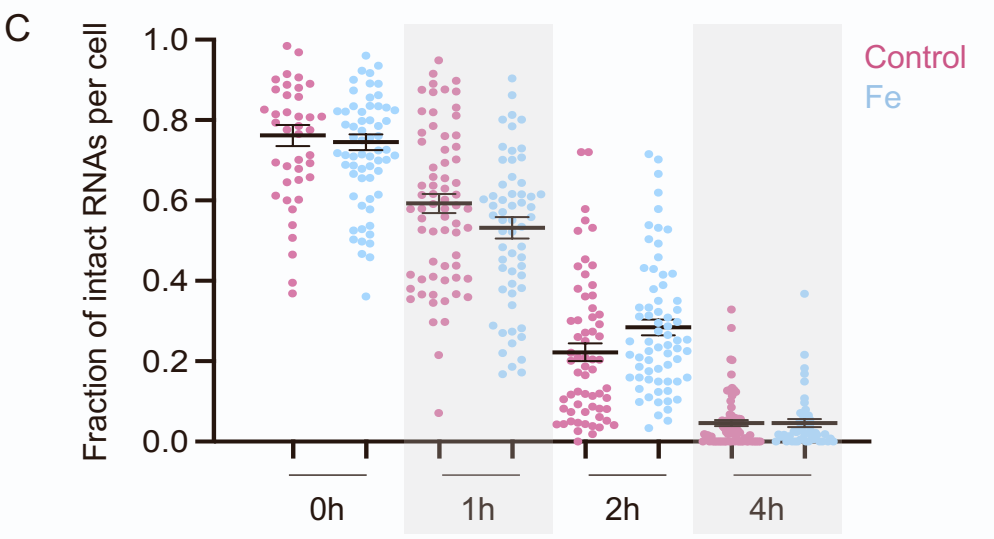

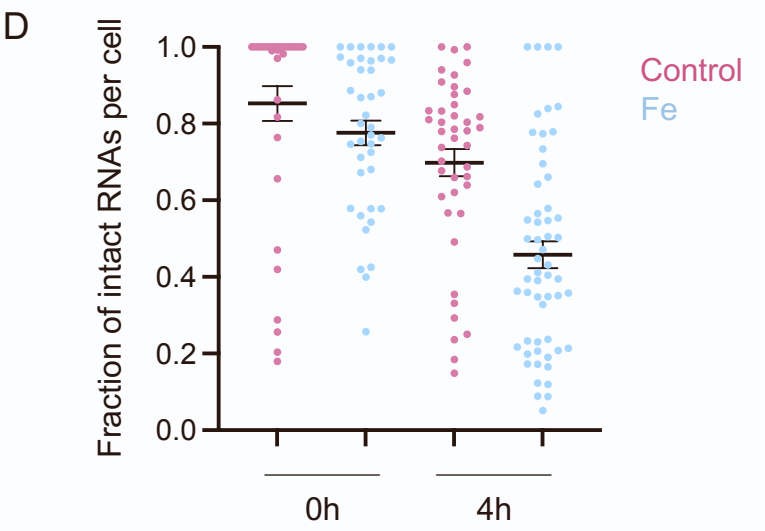

Figure S5. Iron treatment does affect the decay of TREAT mRNAs. Related Figure 2.

A. Schematic representation of TREAT mRNA used to study translation upon treatment of cells with iron. smFISH probes targeting Renilla in ORF (upstream PKs) and MS2 stem-loops in 3'UTR (downstream PKs) is indicated.
B. Representative smFISH images of cells expressing TREAT reporters in presence or absence of iron at indicated time points. Dual-labelled Renilla (green) and MS2 (magenta) spots indicate the intact reporter mRNAs and single-labelled MS2 spots represent stabilized intermediates indicating degraded mRNA.
C. Quantification of mRNA decay from the smFISH images. The fraction of intact mRNAs is shown at indicated time points. Each dot represents the fraction of intact mRNAs per cell, for control (at least 50 cells per time point) and iron-treated cells (at least 50 cells per time point).
D. Quantification of fraction of intact mRNAs per cell of the IRE-TREAT mRNA in control and iron-treated U2OS cells. Mean± SEM

Figure S6

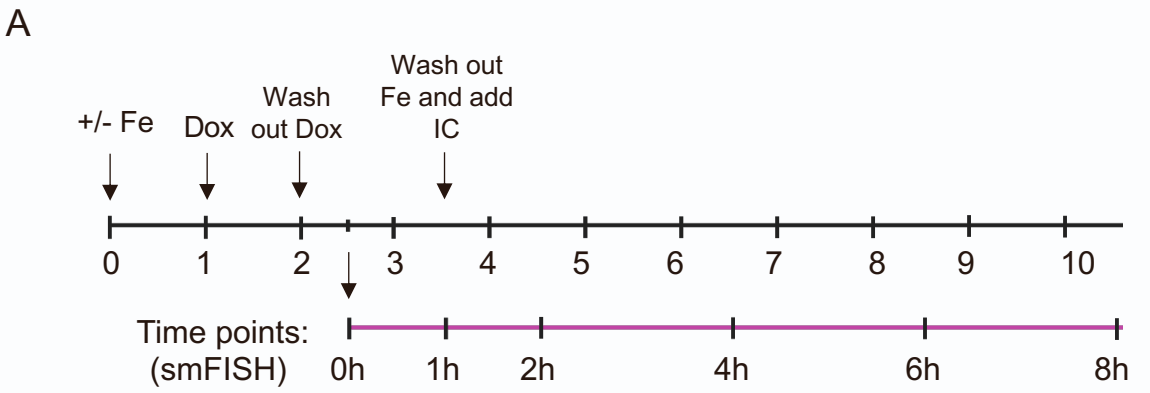

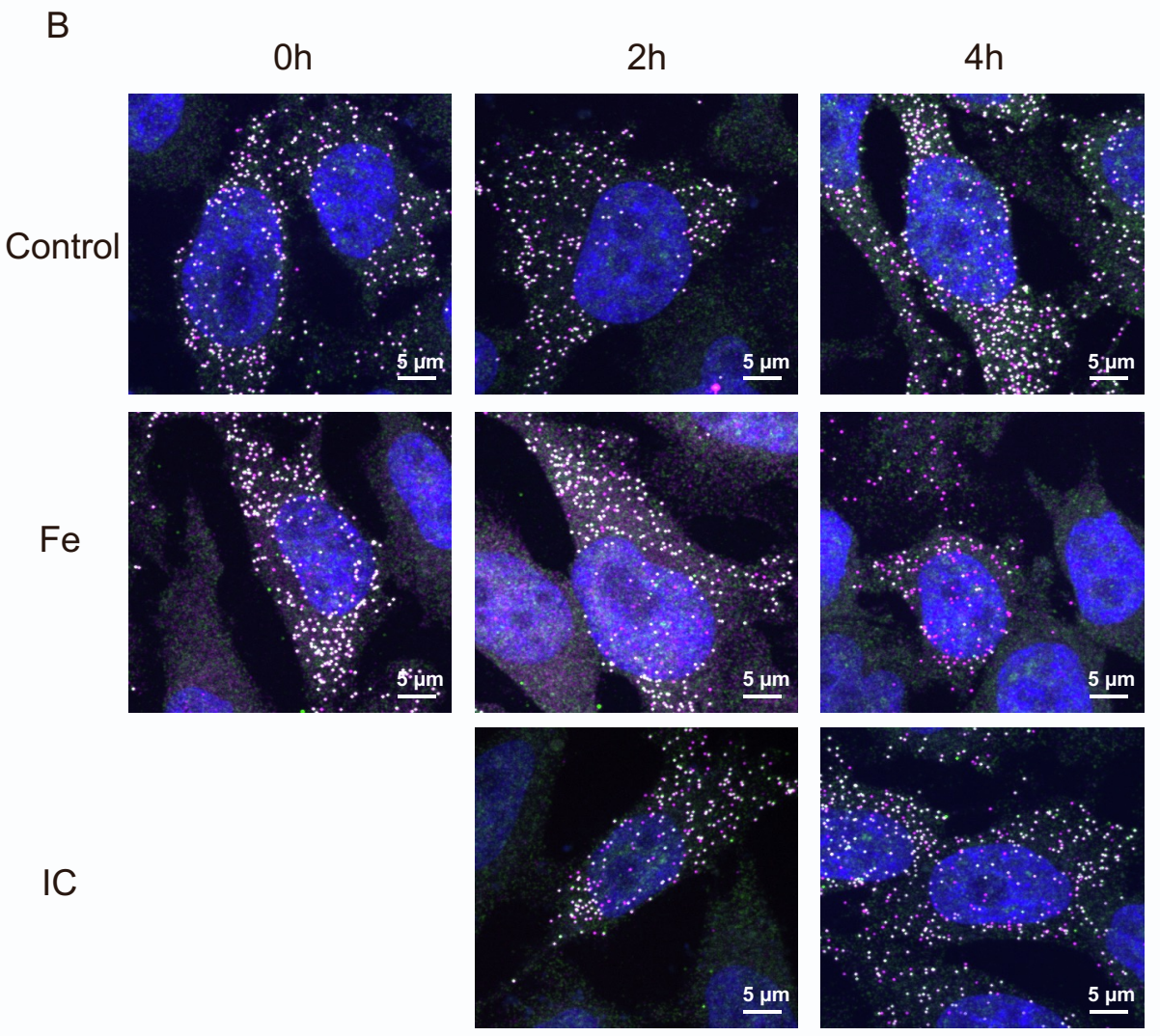

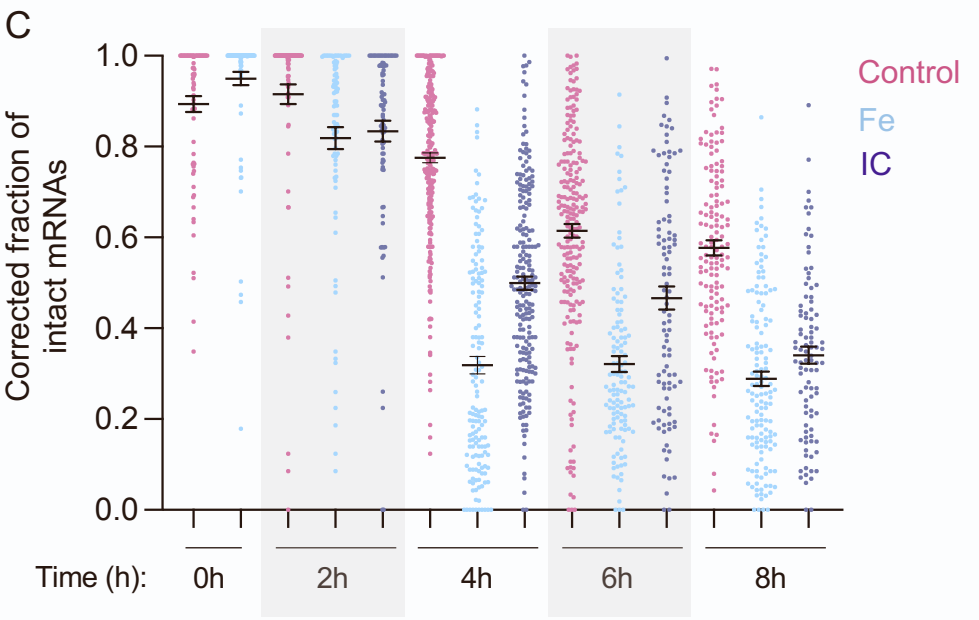

Figure S6. Translation-dependent decay of IRE-TREAT mRNAs is reversible. Related to Figure 2.

A. Schematic representation of the experimental protocol used to study the effect of translation on stability of IRE-TREAT mRNAs. At 1h time point, iron was washed out and IC was added to the culture medium. The stability of untreated cells (control), Fe-treated cells (Fe) and iron chelator-treated cells (IC) was measured by smFISH at indicated time points.

B. Representative smFISH images of cells expressing IRE-TREAT mRNAs at indicated time points. Dual-labelled Renilla (green) and MS2 (magenta) spots indicate intact reporter mRNAs and single-labelled MS2 (magenta) spots represent stabilized intermediates indicating degraded mRNA.

C. Quantification of mRNA decay from the smFISH images. The fraction of intact mRNAs is indicated at each time point. Mean± SEM

Figure S7

A

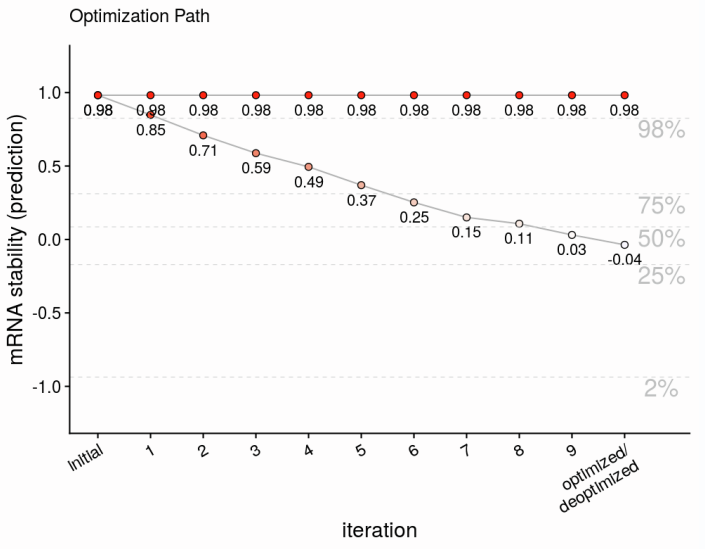

B

```
Optimal          1 ATGGCTTCCAAGGTGTACGACCCCGAGCAACGCAAACGCATGATCACTGG     50
                   ||||||...|||||||||||||||||||.|.||||||||||||||||||
Non-optimal      1 ATGGCTAGTAAGGTGTACGACCCCGAGCAAAGGAAACGCATGATCACTGG     50

Optimal         51 GCCTCAGTGGTGGGCTCGCTGCAAGCAAATGAACGTGCTGGACTCCTTCA    100
                   |||.||.|||||||||.|.||||||.|||||||||||||||||||||||||
Non-optimal     51 GCCACAATGGTGGGCTAGGTGCAAACAAATGAACGTGCTGGACTCCTTCA    100

Optimal        101 TCAACTACTATGATTCCGAGAAGCACGCCGAGAACGCCGTGATTTTTCTG    150
                   |.||||||||||||....|||||||||||||||||||||||||..||..|.
Non-optimal    101 TAAACTACTATGACAGTGAGAAGCACGCCGAGAACGCCGTGATATTCTTA    150

Optimal        151 CATGGTAACGCTGCCTCCAGCTACCTGTGGAGGCACGTCGTGCCTCACAT    200
                   |||||.||||||||||||||||.|||||||||||||||.||||||.||||||
Non-optimal    151 CATGGGAACGCTGCCTCCAGCTATCTGTGGAGGCACGTAGTGCCGCACAT    200

Optimal        201 CGAGCCCGTGGCTAGAtgcatcatccctgatctgatcggaatgggtaagt    250
                   .||.||||||||.||||||||||.|||||||.||||.|||||||||||||||
Non-optimal    201 TGAACCCGTGGCGAGATGCATCATACCTGATTTGATAGGAATGGGTAAGT    250

Optimal        251 ccggcaagagcgggaatggctcatatcgcctcctggatcactacaagtac    300
                   |||||||.||||||||||||...|||||||||||||||||||||||.|||
Non-optimal    251 CCGGCAAAAGCGGGAATGGCAGCTATCGCCTCCTGGATCACTACAAATAC    300

Optimal        301 ctcaccgcttggttcgagctgctgaaccttccaaagaaaatcatctttgt    350
                   .|.||.||.||||||||.|||.|.||||||||.||.||||||||.||||||
Non-optimal    301 TTAACTGCGTGGTTCGAACTGTTAAACCTTCCGAAAAAAATCATTTTTGT    350

Optimal        351 gggccacgactgggggggcttgtctggcctttcactactcctacgagcacc    400
                   |||.|||||||||||||||.|||.|.||||||||||...||||||||||
Non-optimal    351 GGGGCACGACTGGGGGGCGTGTTTAGCCTTTCACTACAGTTACGAGCACC    400

Optimal        401 aagacaagatcaaggccatcgtccatgctgagagtgtcgtggacgtgatc    450
                   ||||||||||.||||||.||||||||||.||||||||.||||||||||.
Non-optimal    401 AAGACAAGATAAAGGCGATCGTCCATGCGGAGAGTGTGGTGGACGTGATA    450

Optimal        451 gagtcctgggacgagtggcctgacatcgaggaggatatcgccctgatcaa    500
                   |||..|||||||||||||||.||||||.||||||||.||.||..|.||||||
Non-optimal    451 GAGAGCTGGGACGAGTGGCCCGACATTGAGGAGGACATAGCGTTAATCAA    500

Optimal        501 gagcgaagagggcgagaaaatggtgcttgagaataacttcttcgtcgaga    550
                   |...|||||||||||||||||||||||||||||||||||.||||||.||||
Non-optimal    501 GTCGGAAGAGGGCGAGAAAATGGTGCTTGAGAATAATTTCTTTGTAGAGA    550

Optimal        551 ccatgctcccaagcaagatcatgcggaaactggagcctgaggagttcgct    600
                   ||||||||||.||||||||.|||.||||||.|.|||||||||||||||||.
Non-optimal    551 CCATGCTCCCCAGCAAGATAATGAGGAAATTAGAGCCTGAGGAGTTCGCG    600

Optimal        601 gcctacctggagccattcaaggagaagggcgaggttagacggcctaccct    650
                   |||||.||.||||||||||||||.||||||||||.|||.||||.||..|
Non-optimal    601 GCCTATCTAGAGCCATTCAAGGAAAAGGGCGAGGTAAGAAGGCCGACGTT    650

Optimal        651 ctcctggcctcgcgagatccctctcgttaagggaggcaagcccgacgtcg    700
                   ...||||||||||||.||.||||||||||.|||||||||||||||||||||
Non-optimal    651 GAGCTGGCCTCGCGAAATTCCTCTCGTTAAAGGAGGCAAGCCCGACGTCG    700

Optimal        701 tccagattgtccgcaactacaacgcctaccttcgggccagcgacgatctg    750
                   ||||||||||..|.||||||||||.||.||||||||.||||||||||||||
Non-optimal    701 TCCAGATTGTTAGGAACTACAACGCGTATCTTCGGGCGAGCGACGATCTG    750

Optimal        751 cctaagatgttcatcgagtccgaccctgggttcttttccaacgctattgt    800
                   |||||.||||||||.|||...||||||||||.||||..||||||||||||
Non-optimal    751 CCTAAAATGTTCATAGAGAGTGACCCTGGGTTTTTTAGCAACGCTATTGT    800

Optimal        801 cgagggagctaagaagttccctaacaccgagttcgtgaaggtgaagggcc    850
                   .|||||.|||||.||||||||.|||||.|||||.||||||||||||.|||.
Non-optimal    801 AGAGGGGGCTAAAAAGTTCCCGAACACTGAGTTTGTGAAGGTGAAAGGCT    850

Optimal        851 tccacttcagccaggaggacgctccagatgaaatgggtaagtacatcaag    900
                   |.||.||||||||||||||||.||||||||||||||.|||||||||
Non-optimal    851 TACATTTCAGCCAGGAGGACGCTCCGGATGAAATGGGTAAATACATCAAG    900

Optimal        901 agcttcgtggagcgcgtgctgaagaacgagcag---    933
                   ||||||||||||..|.||||||||||||||||||
Non-optimal    901 AGCTTCGTGGAAAGAGTGCTGAAGAACGAGCAGTAA    936
```

C

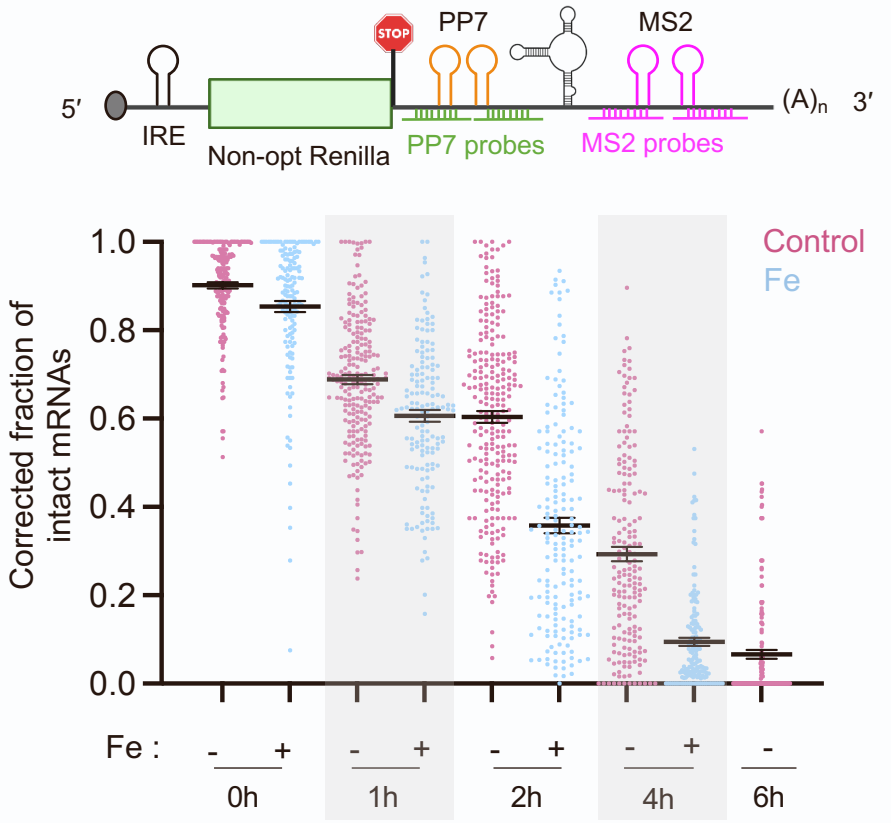

Figure S7. Translation-dependent degradation of mRNAs containing non-optimal codons in the ORF. Related to Figure 2.

A. Codon-optimality of the Renilla luciferase sequence in the IRE-TREAT mRNAs. The input sequence remained unchanged even after 10 iterations of codon optimization indicating the sequence is already codon-optimized. The non-optimal Renilla luciferase sequence was obtained after 10 rounds of deoptimization.
B. Sequence alignment of the optimal and non-optimal Renilla luciferase sequence. The number of nucleotides changed was 120 and the number of codons changed was 93. The non-optimal codons are uniformly distributed throughout the sequence.
C. Schematic of the non-opt-IRE-TREAT encoding Renilla luciferase and its degradation kinetics in untreated and iron-treated cells (as per the timeline in Figure 2B). The fraction of intact mRNAs is shown for the indicated time points. The non-optimal-IRE TREAT mRNAs is degraded faster as compared to IRE-TREAT mRNAs containing optimal codons.

Figure S8

A

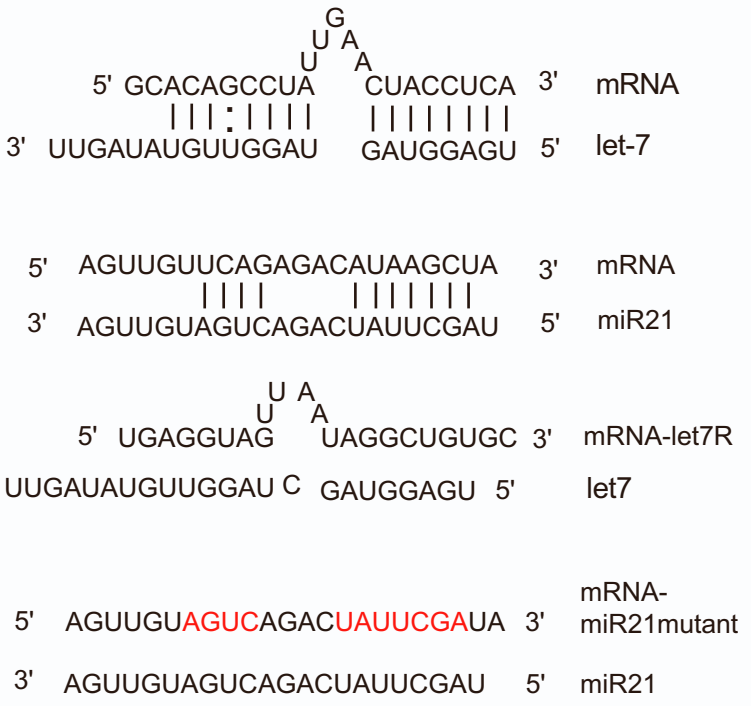

B

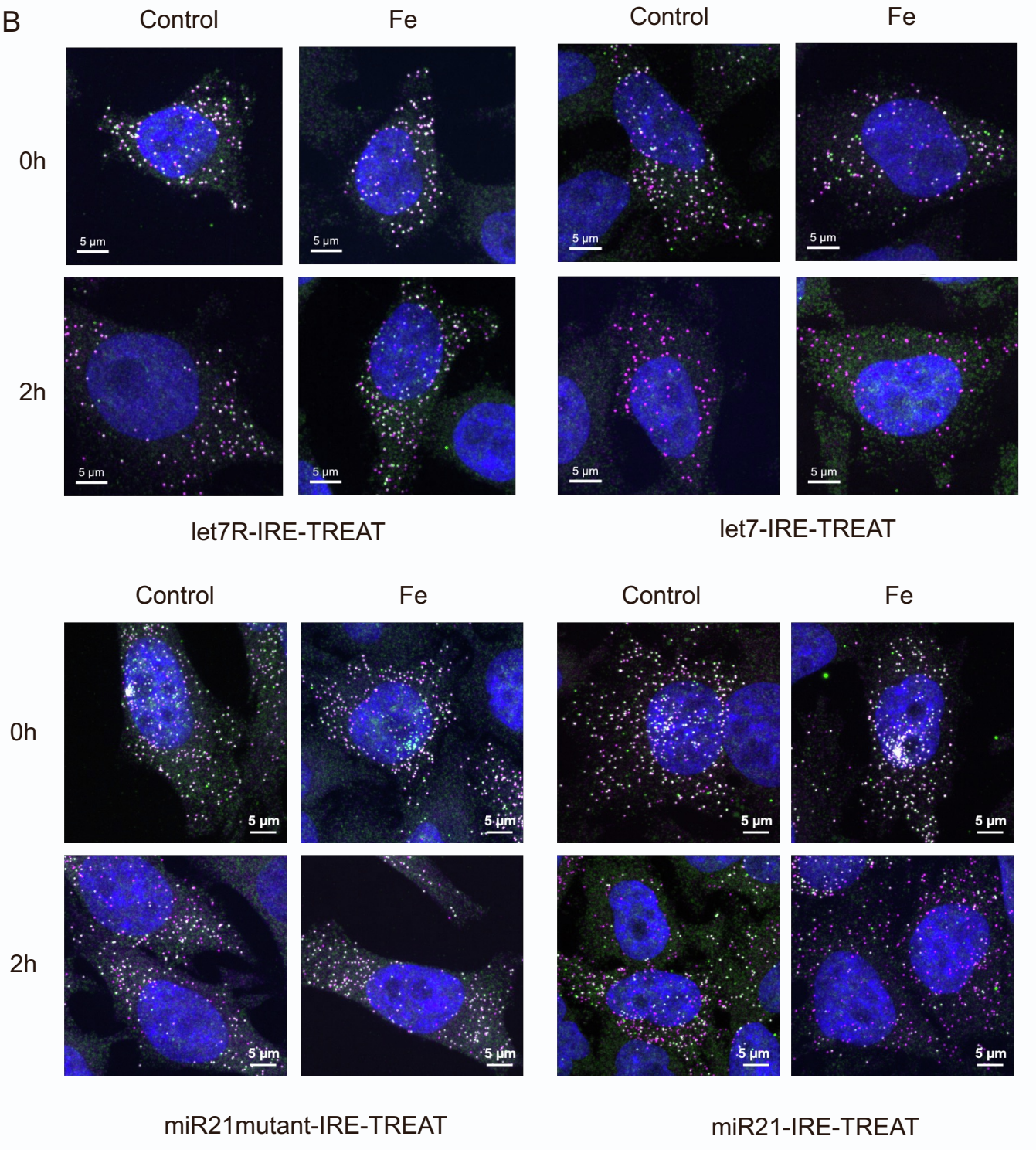

C

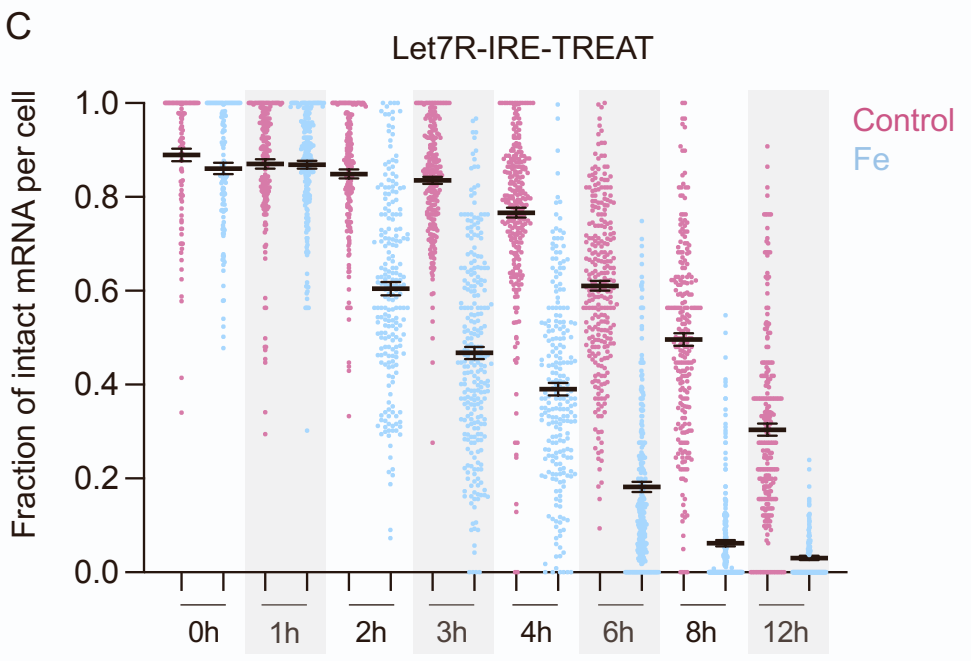

E

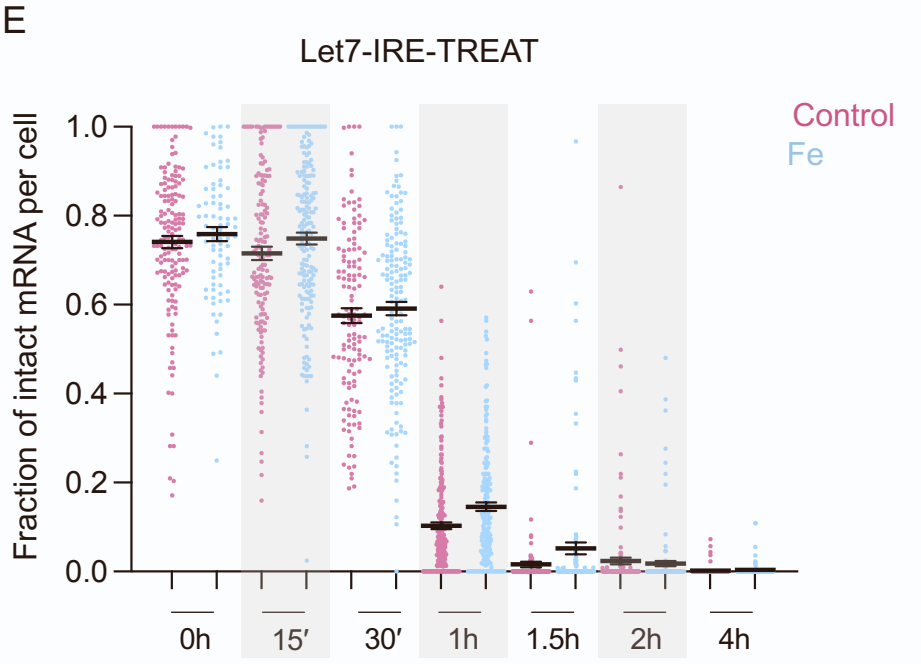

D

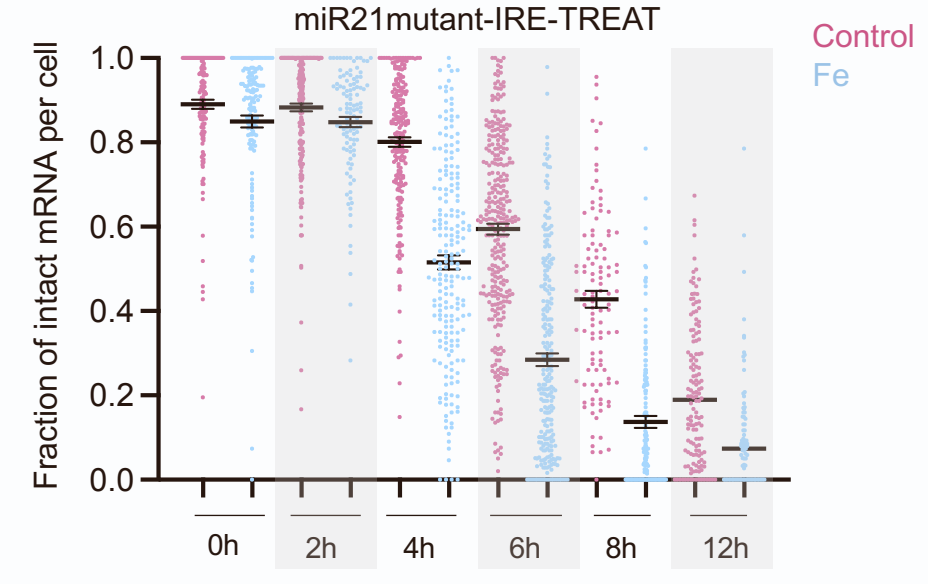

F

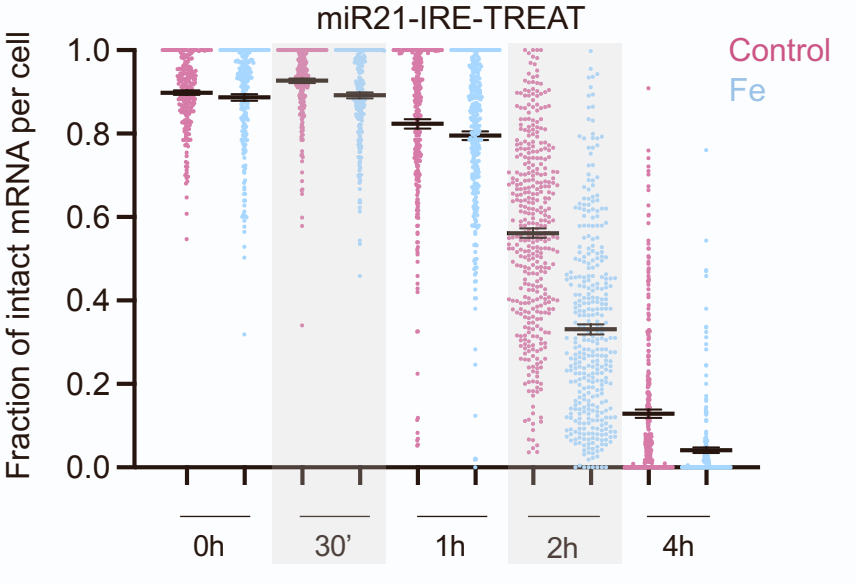

Figure S8. Decay kinetics of miRNA- IRE-TREAT mRNAs. Related to Figure 6.

A. Sequence of miRNA binding sites in the miRNA-IRE-TREAT mRNAs used in this study. Vertical lines indicate base pairing between the miRNA and the mRNA. For the let7R control reporter, the let7 binding sites were reversed. Whereas for the miR21mutant control, the seed sequence in the miR21 binding site was mutated.
B. Representative smFISH images of cells expressing miRNA-IRE-TREAT mRNAs, in the presence or absence of iron, at indicated time points. Dual-labelled Renilla (green) and MS2 (magenta) spots represent intact intact mRNAs and single-labelled MS2 (magenta) spots indicate stabilized intermediates, representing degraded mRNAs.
C. Quantification of mRNA decay from the smFISH images of cells expressing let7R-IRE-TREAT mRNAs. The fraction of intact mRNAs is shown at the indicated time points. Mean±SEM
D. Quantification of mRNA decay from the smFISH images of cells expressing miR21mutant-IRE-TREAT mRNAs. The fraction of intact mRNAs is shown at the indicated time points. Mean±SEM.
E. Quantification of mRNA decay from the smFISH images of cells expressing let7-IRE-TREAT mRNAs. The fraction of intact mRNAs is shown at the indicated time points. Mean±SEM.
F. Quantification of mRNA decay from the smFISH images of cells expressing miR21-IRE-TREAT. The fraction of intact mRNAs is shown at the indicated time points. Mean±SEM.

Figure S9

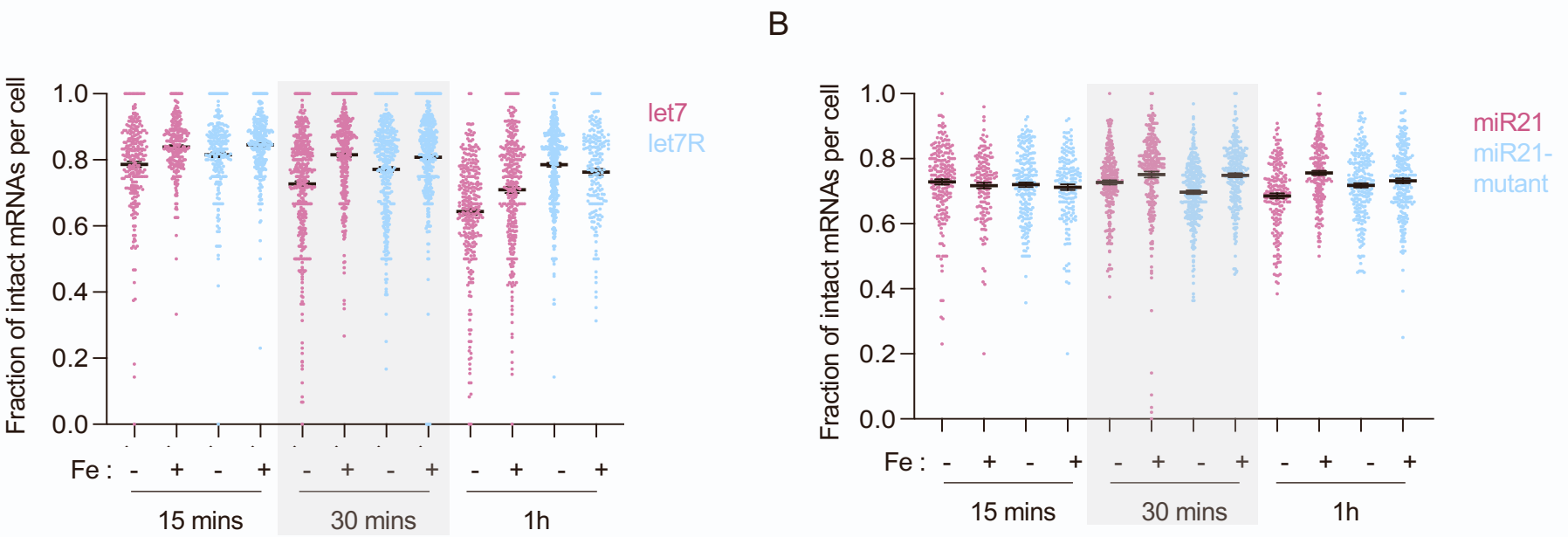

Figure S9. miRNA-mediated regulation of translation and decay by three-color single-molecule imaging. Related to Figure 7.

A. Quantification of the fraction of intact mRNAs per cell for let7-IRE-SunTag-TREAT and let7R-IRE-SunTag-TREAT mRNAs, in untreated (maroon) or iron-treated cells (blue).

B. Quantification of the fraction of intact mRNAs per cell for miR21-IRE-SunTag-TREAT and miR21mutant-IRE-SunTag-TREAT mRNAs, in untreated (maroon) or iron-treated cells (blue).

C. Live-cell single-molecule imaging of let7-IRE-SunTag-TREAT and let7R-IRE-SunTag-TREAT mRNAs in untreated cells and cells treated with iron for 2 hours. The mRNAs were induced with doxycycline for 2 hours before imaging. mRNAs (magenta) undergoing translation co-localize with the SunTag (green) signal.

D. Live-cell single-molecule imaging of miR21-IRE-SunTag-TREAT and miR21mutant-IRE-SunTag-TREAT mRNAs in untreated cells and cells treated with iron for 2 hours. The mRNAs were induced with doxycycline for 2 hours before imaging. mRNAs (magenta) undergoing translation co-localize with the SunTag (green) signal.

E. Schematic representation of let7-SunTag and let7R-SunTag mRNAs used to perform live-cell imaging of miRNA regulated mRNA translation.

F. Representative image from the live-cell single-molecule imaging of let7-SunTag and let7R-SunTag mRNAs. The mRNA was induced with doxycycline for 2 hours. mRNAs (magenta) undergoing translation co-localize with the SunTag (green) signal.

G. The distribution of fraction of translating mRNAs per cell from 4 independent experiments. n.s. indicates not significant. Color-coded dots represent averages from individual experiments.

Single-molecule imaging reveals translation-dependent destabilization of mRNAs

Methods S1. Detailed description of mathematical modeling. Related to Figures 3-6 and STAR Methods

Pratik Dave, Gregory Roth , Esther Griesbach, Daniel Mateju and Jeffrey A. Chao

Contents

In this Supplementary Information we describe the different mathematical models used in the study, their analysis and the fitting procedure.

1 Mathematical model for translation

Translation occurs in intermittent bursts of ribosome initiation. This bursty behavior can be described by a delay two-state model in which the mRNA stochastically switches between an off state and an on state where translation can initiate.

1.1 Delay two-state model for translating ribosome per RNA

The two-state model was first introduced to describe the turnover of mRNAs (Peccoud and Ycart, 1995). The delay two-state model was introduced later to describe the turnover of RNA polymerases II (Pol II) actively transcribing a gene (Xu et al., 2016). The delay arises from the fact that elongation and termination are not first-order reactions but rather deterministic processes lasting for a fixed time that is interpreted as a delay of the termination reaction. Here we use the same model to describe the number of translating ribosomes per RNA. We assume that a RNA stochastically switches between an *off* state (inactive) and an *on* state (active) where initiation of a ribosome can occur. The transitions between those states occur with rates k_{on} and k_{off}. Initiation of ribosomes is regarded as a Poisson process and occur at rates μ. The elongation time is determined by the open reading frame length, L, and the translation elongation speed that we set to 4 amino acids per second, that is $t_{elong} = \frac{L}{4}$.

There is an analytical expression of the steady-state distribution of the delay two-state model (Xu et al., 2016; Fu et al., 2022) but its computation required high precision evaluation. Here, we follow Fu et al., 2022, and calculate the steady-state probability distribution of the delay two-state model by using the finite state projection algorithm (Gupta, Mikelson, and Khammash, 2017). This method consists of truncating the infinite state space of the system into a finite subset of states in order to reduce the infinite-dimensional system of ODEs into a finite system. Here, the truncation consists in fixing a maximal number of translating ribosomes per RNA which we set to 120% of the maximal number observed in the SunTag experiment. The code for these calculations was written in Matlab (version 2019b) and are available on Github (`https://github.com/gregroth/TransDegModels`).

1.2 Delay two-state model fitting

The delay two-state model described above was fit to the distributions of ribosome numbers inferred from the SunTag experiments. This section describes in detail how this was done. In the sequel, all the rates are expressed in unit of 1 over the ribosome elongation time.

For each condition, we calculated the histogram, $\mathbf{h}$ of the ribosome counts obtained from the SunTag experiment. The bin size b was set to 1.

For each set of parameters $\boldsymbol{\theta} = (k_{on}, k_{off}, \mu)$ we calculated the steady-state probability distributions of the corresponding delay two-state model. Next, we discretised the steady-state distributions in a histogram $\boldsymbol{\eta}(\boldsymbol{\theta})$ which is comparable with the histogram $\mathbf{h}$ obtained from the SunTag data. We assume that the count in bin i follows a binomial distribution of mean $\eta_i N$ and variance $\eta_i(1-\eta_i)N$, where N is the total number of counts. We approximate the binomial

distribution by a normal distribution. Hence, the likelihood of observing the histogram $\mathbf{h}$ given the parameters $(\boldsymbol{\theta})$ is

$$L(\boldsymbol{\theta}) = \prod_{i=1}^{n_b} \frac{1}{\sqrt{2\pi N \eta_i (1-\eta_i)}} e^{-\frac{(h_i - \eta_i(\boldsymbol{\theta}))^2}{2\eta_i(1-\eta_i)N}} \tag{1}$$

and the log likelihood is

$$LL(\boldsymbol{\theta}) = \sum_{i=1}^{n_b} \left[-\frac{(h_i - \eta_i(\boldsymbol{\theta}))^2}{2\eta_i(1-\eta_i)N} + \frac{1}{2}\log(2\pi N \eta_i(1-\eta_i)) \right] \tag{2}$$

The best fit parameter maximises the log likelihood function LL. We set a lower bound of 0 for all the parameters and an upper bound of 1000 for the parameters k_{on}, k_{off}, μ. We ensured that the best fit parameters found were not at the boundaries. For all the maximisations we use a global search approach. Specifically, we use the Matlab function *MultiStart* in the *Global Optimization* toolbox. All codes were written in Matlab (version 2019b) and are available at `https://github.com/gregroth/TransDegModels`.

1.3 Profile likelihood analysis and confidence interval

We calculated the profile likelihood of all the parameters and derived their confidence intervals (see e.g. Pawitan, 2001). Let us denote $\boldsymbol{\theta} = (k_{on}, k_{off}, \mu)$ such that θ_j corresponds to the jth parameter (e.g. θ_2 corresponds to k_{off}). The profile likelihood function of parameter j is

$$PL_j(x) = \max_{\boldsymbol{\theta}|\theta_j = x} LL_{tot}(\boldsymbol{\theta}), \tag{3}$$

i.e. for each value x of parameter j the log-likelihood is maximised over the other parameters. The 95% confidence interval of parameter j is

$$CI_j = \{x | LL_{tot}(\boldsymbol{\theta}^*) - PL_j(x) \leq 1.9207\} \tag{4}$$

where $\boldsymbol{\theta}^* = \arg\max_{\boldsymbol{\theta}} LL(\boldsymbol{\theta})$ and 1.9207 is half of the $.95$-quantile of the chi squared distribution with one degree of freedom. The profile likelihood functions were estimated using the Matlab function *MultiStart* in the *Global Optimization* toolbox.

2 Mathematical models for RNA degradation

Degradation of mRNA can be coupled to translation in various ways. Degradation could depend on the *flux* of ribosomes on the template, or, alternatively, degradation could depend on the *presence* of ribosomes undergoing elongation on the template. Here, we define mathematical models that describe these two ways of coupling translation and degradation of mRNAs.

2.1 Ribosome-flux dependent degradation

In this Section, we assume that degradation is dependent on the flux of ribosomes on the template. We consider three models. The first model assumes that degradation occurs with a fixed probability after each initiation (or termination) event. The second model assumes that degradation occur after each initiation (or termination) event with a probability that increases with the number of initiation (or termination) events. Finally, the third model assumes that degradation occurs with a rate that depends on the number of initiation events.

2.1.1 Fixed probability to degrade after each initiation event

The first model that we consider assumes that degradation of the mRNA molecule can be trigger at each initiation (or termination) event with a fixed probability. The model is fully stochastic and describes the time evolution of an RNA molecule defined by three variables: the nucleus/cytoplasm state, the translation state, and the RNA life state. The nucleus/cytoplasm state is $\mathcal{C}_0$ if the RNA is in the nucleus and it is $\mathcal{C}_1$ if it is in the cytoplasm. The translation states describe the translational activity of the RNA ($\mathcal{P}_0$ if the RNA cannot initiate translation; $\mathcal{P}_1$ if the RNA is prone to initiate translation). Finally, the RNA life states describe the life status of the RNA molecule. The life state is $\mathcal{I}_0$ if the RNA has been degraded and it is $\mathcal{I}_1$ if the RNA has not been degraded yet. We assume that the transition between nucleus state and cytoplasm state is irreversible. The transitions between the *on* and *off* state of the RNA are reversible. Translation can only be initiated from the RNA state $\mathcal{P}_1$ (i.e *on* state). Degradation of the RNA molecule occurs with a fixed probability, p_δ, after each initiation event. The kinetic reactions are as follows.

$$\begin{aligned} \mathcal{C}_0 &\underset{\gamma}{\rightarrow} \mathcal{C}_1 \\ \mathcal{C}_1 + \mathcal{P}_0 &\underset{k_{on}}{\overset{k_{off}}{\rightleftharpoons}} \mathcal{C}_1 + \mathcal{P} \\ \mathcal{C}_0 + \mathcal{P}_1 &\underset{\mu}{\rightarrow} \mathcal{C}_0 + \mathcal{P}_1 + \mathcal{E} \overset{p_\delta}{\rightsquigarrow} \mathcal{I}_0 \end{aligned}$$

where $\mathcal{E}$ represents a new initiation event and $\rightsquigarrow$ represents the initiation-mediated degradation that occurs with probability p_δ. We implement the initiation-mediated degradation manually in the Gillespie algorithm. After each time the initiation reaction occurs, we draw a random number $r \in [0, 1]$ and degrade the mRNA if $r \leq p_\delta$.

Biological interpretation: this model assumes that the initiation (or termination) of a ribosome on the template triggers the degradation of the mRNA. Hence, under this model, degradation can not occur when no ribosome is engaged on the template. Note that, under this assumption, degradation is a memory less process: the probability that an initiation event triggers degradation is independent on the number of initiation that have already occurred.

2.1.2 Increasing probability to degrade after each initiation event

The second model that we consider assumes that degradation of the mRNA molecule can be triggered after each initiation (or termination) event with a probability that increases with the number of initiation events. The model is fully stochastic and describes the time evolution of an RNA molecule defined by four variables: the nucleus/cytoplasm state, the translation state, the RNA life state, and the number of initiation events. The three first variables are defined as in Section 2.1.1. The number of translation initiation events can be any integer $N \geq 0$. Degradation of the RNA molecule occurs after each initiation event with probability $p_\delta(N)$. The function $p_\delta(\cdot)$ describes the relationship between the initiation-mediated degradation probability and the number of initiation events. We define the function $p_\delta(\cdot)$ as follows.

$$p_\delta(N) = 1 - e^{-\delta_0 N t_{elong}}, \tag{5}$$

where δ_0 is the magnitude of increment in the rate of degradation. Equation (5) corresponds to the probability that an mRNA is degraded per ribosome if degradation was a first-order reaction with rate $\delta_0 N$, as in model 2.1.3. The kinetic reactions are as follows.

$$
\begin{aligned}
\mathcal{C}_0 &\underset{\gamma}{\rightarrow} \mathcal{C}_1 \\
\mathcal{C}_1 + \mathcal{P}_0 &\underset{k_{on}}{\overset{k_{off}}{\rightleftharpoons}} \mathcal{C}_1 + \mathcal{P} \\
\mathcal{C}_0 + \mathcal{P}_1 &\underset{\mu}{\rightarrow} \mathcal{C}_0 + \mathcal{P}_1 + \mathcal{E} \overset{p_\delta(N)}{\rightsquigarrow} \mathcal{I}_0
\end{aligned}
$$

where $\mathcal{E}$ represents a new initiation event, $\rightsquigarrow$ represents the initiation-mediated degradation that occurs with probability $p_\delta(N)$. We implement the initiation-mediated degradation manually in the Gillespie algorithm. After each time the initiation reaction occurs, we draw a random number $r \in [0, 1]$ and degrade the mRNA if $r \leq p_\delta(N)$.

Biological interpretation: as for model 2.1.1, this model assumes that the initiation (or termination) of a ribosome triggers the degradation of the mRNA. Hence, under this model, degradation can not occur when no ribosome is engaged on the template. In contrast with model 2.1.1, this model assumes that degradation is a memory process: the more ribosome initiation events have occurred, the more likely the degradation will be trigged by a ribosome initiation.

2.1.3 Degradation rate dependent on the ribosome flux

The third model that we consider assumes that degradation is a first-order reaction with a rate that is proportional to the number of ribosomes that have translated the mRNA. The model is fully stochastic and describes the time evolution of an RNA molecule defined by four variables: the nucleus/cytoplasm state, the translation state, the RNA life state, and the number of initiation events. The three first variables are defined as in Section 2.1.1. The number of translation initiation events can be any integer $N \geq 0$. Degradation of the RNA molecule occurs with a rate that increases linearly with the number of initiation events. The magnitude of increment in the rate of degradation is δ_0. The kinetic reactions are as follows.

$$
\begin{aligned}
\mathcal{C}_0 &\underset{\gamma}{\rightarrow} \mathcal{C}_1 \\
\mathcal{C}_1 + \mathcal{P}_0 &\underset{k_{on}}{\overset{k_{off}}{\rightleftharpoons}} \mathcal{C}_1 + \mathcal{P}_1 \\
\mathcal{C}_0 + \mathcal{P}_1 &\underset{\mu}{\rightarrow} \mathcal{C}_0 + \mathcal{P}_1 + \mathcal{E} \\
\mathcal{I}_1 &\underset{\delta_0 N}{\rightarrow} \mathcal{I}_0
\end{aligned}
$$

where $\mathcal{E}$ represents a new initiation event.

Biological interpretation: this model assumes that the passage of a ribosome on the template "destabilises" the mRNA, leading to an increase in the degradation rate. The difference with models 2.1.1 and 2.1.2, is that ribosome passage destabilises the mRNA but doesn't necessary triggers degradation. Therefore, in this model, degradation might occur at any time. Importantly, this model assumes that degradation is a memory process: the more ribosome initiation events have occurred, the more likely degradation will occur.

2.2 Ribosome-number dependent degradation

The fourth model that we consider assumes that degradation is dependent on the presence of ribosomes on the template. We assume that degradation is a first-order reaction with a rate that is proportional to the number of ribosomes elongating on the template. Such a model must describe the ribosome dynamics for each RNA molecule. The model is fully stochastic and describes the time evolution of an RNA molecule defined by four variables: the nucleus/cytoplasm state, the translation state, the RNA life state, and the number of elongating ribosomes. The number of elongating ribosomes can be any integer $r \geq 0$ and the other variables are defined as in Section 2.1.1. Degradation of the RNA molecule occurs with a rate that linearly increases with the number of ribosomes elongating on the template. The magnitude of increment in the rate of degradation is δ_0. The kinetic reactions are as follows.

$$
\begin{aligned}
\mathcal{C}_0 &\underset{\gamma}{\rightarrow} \mathcal{C}_1 \\
\mathcal{C}_1 + \mathcal{P}_0 &\underset{k_{on}}{\overset{k_{off}}{\rightleftharpoons}} \mathcal{C}_1 + \mathcal{P}_1 \\
\mathcal{C}_0 + \mathcal{P}_1 &\underset{\mu}{\rightarrow} \mathcal{C}_0 + \mathcal{P}_1 + \mathcal{R} \text{ triggers } \mathcal{R} \underset{t_{elong}}{\Rightarrow} \emptyset \\
\mathcal{I}_1 &\underset{\delta_0 r}{\rightarrow} \mathcal{I}_0
\end{aligned}
$$

where $\mathcal{R}$ represents a new translating ribosome and $\mathcal{R} \underset{t_{elong}}{\Rightarrow} \emptyset$ represents the termination event that occurs with a delay corresponding to the elongation time t_{elong}.

Biological interpretation: this model assumes that the more ribosomes are on the template, the more likely degradation will occur. As in model 2.1.3 degradation can occur at any time and not only when a ribosome initiates or terminates translation. However, this model assumes that degradation is a memory less process: the degradation rate is independent on the history of the mRNA but depends only on the current number of ribosome on the template.

2.3 Simulation of the RNA degradation models

The initial population of mRNA molecules in the experimental data contains m_0^c cytoplasmic mRNAs, m_0^n nuclear mRNAs and m_0^s stabilised $3'$ degradation intermediates. We simulate the time evolution of each RNA molecule separately using the Gillespie algorithm (Gillespie, 1977) and its adaptation for models with delay (Barrio et al., 2006) in the case of the ribosome-presence-dependent degradation model. The initial condition for a nuclear mRNA is 1 for the nucleus/cytoplasm state and 0 for the other variables. Each cytoplasmic mRNA might have different initial condition as it might have already started translation at time 0. For the models that are memory less, we assume that the initial condition for a cytoplasmic mRNA is 0 for all the variables (i.e. we assume it is in the OFF state). For the models with memory (i.e. the number of passage affects the degradation), we assume that each cytoplasmic mRNA molecule comes from a transcription burst that on average happened 30 minutes after starting induction (i.e. 1 hours before time 0). Therefore, each cytoplasmic mRNA is simulated from time -1 hour with an initial condition corresponding to 1 for the nucleus/cytoplasm state and 0 for the other variables. We simulate 1000 times the trajectory of each RNA separately and we calculate

the time evolution of the mean number of RNA molecules $\bar{M}(t)$ as follows,

$$\bar{M}(t) = \frac{1}{1000} \sum_{i=1}^{1000} x_i(t), \tag{6}$$

where $x_i(t)$ is the life state of the RNA molecule i at time t (in the experimental time scale).

All the simulations were made in MATLAB (MathWorks, R2019b).

2.4 Fit of the degradation models

Given a data set, let n be the number of time points $(t_1, \ldots, t_n)$. Let m_i and n_i be the number of cytoplasmic mRNAs and nuclear mRNAs at time t_i, respectively. In all the models, the parameters related to the two-state regime of translation (i.e. k_{on}, k_{off}, and μ) are fixed to their value obtained by the fit of the delay two-state model to the distribution of the ribosome number per mRNA (see Section 1.2). The export rate γ is estimated separately. We fit an exponential function to the number of nuclear mRNA at time points 0, $.25$, $.5$ and 1 hour, averaged among the miR21-IRE-TREAT mRNAs and Let7-IRE-TREAT mRNAs in iron-treated condition. We use least square regression to estimate the export rate.

The rest of the parameters for all the degradation models were estimated by fitting the model to the iron-treated cell data (Fe) set using the least square regression, that is we minimised the sum of the squared deviations

$$S(\theta) = \sum_{i=1}^{n} (m_i - \bar{M}(t_i))^2 \tag{7}$$

We ensured that the best fit parameters found were not at the boundaries. For all the maximisations we use a global search approach. Specifically, we use the Matlab function *MultiStart* in the *Global Optimization* toolbox. All codes were written in Matlab (version 2019b) and are available at `https://github.com/gregroth/TransDegModels`.

2.5 Model selection

The fits of all the degradation models to the IRE-TREAT mRNAs in iron-treated condition were compared using the difference Akaike information criterion (see e.g. Burnham and Anderson, 2002). The difference Akaike information criteria (Δ AIC) are listed in Table 2. The best model is the flux model 2.1.3. In addition, we compared the performances of each model to predict the other 7 data sets where the translation parameters (k_{on}, k_{off}, μ) were replaced by their values obtained by the fits of their respective ribosome distributions and the degradation parameter was fixed to its value obtained from the fit to the IRE-TREAT mRNAs in iron-treated condition. The performance is measured by averaging the standard error (i.e. mean distance between observed values and model prediction) over the 7 data sets. The standard errors of the predictions for each data set are listed in Table 3 and the performances of the predictions (mean S.E. of predictions) are listed in Table 2. Again the best model is clearly the flux model 2.1.3 with an average standard error of 7.23 mRNAs. The model fit and the model predictions for the flux model 2.1.3 are shown in the main figures; the model fit and the model predictions for the other flux models (2.1.1 and 2.1.2) and for the ribosome number model (2.2) are shown in Figures 1,2, and 3, respectively.

2.6 Confidence interval analysis

For each parameter θ we calculate the F test statistics for the test $\theta = \theta^*$ where θ^* is the value of the parameter obtained through the least square estimation. The F test is

$$T_\theta = (n-p)\frac{S(\theta) - S(\theta^*)}{S(\theta^*)} \tag{8}$$

where p is the number of free parameters. The confidence interval is given by the values of θ such that $T < q_{0.95}^{F_{1,n-p}}$, where $q_{0.95}^{F_{a,b}}$ is the 95 percentile of the Fisher distribution with a, b degrees of freedom.

3 Mathematical model for nonsense-mediated degradation

The nonsense-mediated degradation (NMD) mechanism was implemented in our ribosome-flux model (Section 2.1.3) by adding an independent degradation process. Similar to Hoek et al., 2019 we assumed that NMD is induced with a fixed probability, p_{NMD}, after each termination event. We implement the degradation due to NMD manually in the Gillespie algorithm. After each occurrence of the initiation reaction, we draw a random number $r \in [0, 1]$ and degrade the mRNA if $r \leq p_{NMD}$.

Simulation of the full model. The initial population of mRNA molecules in the experimental data contains m_0^c cytoplasmic mRNAs and m_0^n nuclear mRNAs. We simulate the time evolution of each RNA molecule separately using the Gillespie algorithm (Gillespie, 1977). The initial condition for a nuclear mRNA is 1 for the nucleus/cytoplasm state and 0 for the other variables (i.e. $(1, 0, 0, 0)$). We reasoned that NMD-mediated degradation is fast enough such that the cytoplasmic mRNAs have not started yet translation at time 0. Therefore we assumed that the initial condition for a cytoplasmic mRNA is $(0, 1, 0, 0)$.

Importantly, following Hoek et al., 2019, we assumed that 20% of mRNAs are NMD resistant. For each run of simulation, $0.2(m_0^n + m_0^c)$ mRNAs are randomly chosen to be NMD resistant. We simulated their time trajectory using only the basic ribosome-flux model.

Fit of the NMD model. We followed the same fitting procedure that we use for the basic degradation model (see Section 2.4). The only free parameter was the probability that NMD is initiated, i.e. p_{NMD}. All the other parameters were fixed to the best fit values obtained for the IRE-TREAT mRNAs in iron-treated condition (see Section 2.4).

4 Mathematical models for miRNA-mediated degradation

Degradation caused by miRNA on their target mRNA was implemented in our ribosome-flux model (Section 2.1.3) by adding an independent degradation process. We described this process by a single kinetic step. We assumed that this kinetic step depends on the translational status of the mRNA. Hence, we introduced two rates: δ_{mi}^{nontr}, the miRNA-mediated degradation rate when the mRNA is not translating and δ_{mi}^{tr} the miRNA-mediated degradation rate when the mRNA is translating. The kinetic reactions of the full model are as follows.

$$
\begin{array}{rcl}
\mathcal{C}_0 & \underset{\gamma}{\rightarrow} & \mathcal{C}_1 \\
\mathcal{C}_1 + \mathcal{P}_0 & \underset{k_{on}}{\overset{k_{off}}{\rightleftharpoons}} & \mathcal{C}_1 + \mathcal{P}_1 \\
\mathcal{C}_0 + \mathcal{P}_1 & \underset{\mu}{\rightarrow} & \mathcal{C}_0 + \mathcal{P}_1 + \mathcal{E} \\
\mathcal{I}_1 & \underset{\delta_0 f}{\rightarrow} & \mathcal{I}_0 \\
\mathcal{I}_1 + \mathcal{P}_1 & \underset{\delta_{mi}^{tr}}{\rightarrow} & \mathcal{I}_0 + \mathcal{P}_1 \\
\mathcal{I}_1 + \mathcal{P}_0 & \underset{\delta_{mi}^{nontr}}{\rightarrow} & \mathcal{I}_0 + \mathcal{P}_0
\end{array}
$$

where $\mathcal{E}$ represents a new initiation event. The last two reactions represent degradation caused by miRNA.

We also consider a simpler model for which we assume that the miRNA-mediated degradation rate does not dependent on the translation state of the mRNA, i.e. $\delta_{mi}^{nontr} = \delta_{mi}^{tr}$.

Simulation of the miRNA models. The initial population of mRNA molecules in the experimental data contains m_0^c cytoplasmic mRNAs and m_0^n nuclear mRNAs. We simulate the time evolution of each RNA molecule separately using the Gillespie algorithm (Gillespie, 1977). The initial condition for a nuclear mRNA is 1 for the nucleus/cytoplasm state and 0 for the other variables (i.e. $(1, 0, 0, 0)$). We reasoned that miRNA-mediated degradation is fast enough such that the cytoplasmic mRNAs have not started yet translation at time 0. Therefore we assume that the initial condition for a cytoplasmic mRNA is $(0, 1, 0, 0)$.

Fit of the miRNA models and model comparison. We followed the same fitting procedure that we use for the basic degradation model (see Section 2.4). However, in this case we first fit the model using the untreated cell data and then predicted the Fe treated cells data. In the full version of the model, the only free parameters were miRNA-mediated degradation rates, i.e. δ_{mi}^{nontr} and δ_{mi}^{tr}. In the simpler version of the model in which we assumed that the miRNA-mediated degradation was independent on translation, the only free parameter was $\delta_{mi} := \delta_{mi}^{nontr} = \delta_{mi}^{tr}$. In both versions, all the other parameters were fixed to the best fit values obtained for the IRE-TREAT mRNAs in iron-treated condition (see Section 2.4). To compare the two versions of the model, we use the extra sum of squares F-test. The null hypothesis is that the simpler model (the one with fewer parameters) fits the data as well as the more complex model. For both data sets (let7-TREAT and mir21-TREAT), we concludes that the null hypothesis can not be rejected ($p = 0.2$ and $p = 0.4$, respectively).

5 Computing life expectancy of a mRNA molecule

In our model, the life span of a mRNA molecule initiated in the state $(1, 0, 0, 0)$, is defined as the first time its life state is $\mathcal{I}_0$. To estimate the life expectancy of a mRNA molecule, we simulate 1000 mRNA trajectories, all initiated in the state $(1, 0, 0, 0)$ (i.e. as a nuclear RNA) and average their life span.

6 Best fit parameters and model predictions standard error

In this section we provide the best fit parameters for the translation model (Table 1), for the degradation models (Table 2), and for the NMD model and the mircro RNA model (Table 4). We also provide a summary table with the standard errors of the predictions of the different degradation models (Table 3).

Data	Parameter	Best fit value	95% c.i.
IRE-SunTag-Ctrl	Delay-two-state mode		
	k_{on}	6.12	$(5.67, 6.52)$
	k_{off}	18.51	$(17.01, 19.84)$
	μ	71.36	$(70.01, 72.85)$
IRE-SunTag-Fe	Delay-two-state mode		
	k_{on}	6.12	$(5.67, 6.52)$
	k_{off}	3.28	$(2.98, 3.54)$
	μ	71.36	$(70.02, 72.85)$
NoSL-SunTag	Delay-two-state mode		
	k_{on}	18.6	$(17.57, 19.56)$
	k_{off}	22.07	$(20.83, 23.67)$
	μ	222.33	$(220.11, 226.63)$
SL-SunTag	Delay-two-state mode		
	k_{on}	18.6	$(17.57, 19.56)$
	k_{off}	22.07	$(20.83, 23.67)$
	μ	153.3	$(147.4, 159.59)$

Table 1: Best fit parameter values for the two-state model fit to the ribosome distribution measured in SunTag experiment. All the rates are in $1/$hour.

Data	Param.	Best fit value	95% c.i.	S.E. fit	$\triangle$ AIC	mean S.E. of predictions)
IRE-TREAT-Fe	Flux model (2.1.1)					
	p_δ	0.0047	$(0.0037, 0.0075)$	11.9617	33.52	13.97
IRE-TREAT-Fe	Flux model (2.1.2)					
	δ_0	$4.5887e-05$	$(3.4, 6.1)e-05$	4.98	5.75	14.53
IRE-TREAT-Fe	Selected flux model (2.1.3)					
	δ_0	0.0022	$(0.00178, 0.0026)$	4.1425	0	7.23
IRE-TREAT-Fe	Ribosome number model (2.2)					
	δ_0	0.1413	$(0.08, 0.34)$	14.2991	39.22	25.17

Table 2: Best fit parameter values for the degradation models. All the rates are in $1/$hour. Standard error (S.E.) of the fit is the square root of the average squared distance that the observed values fall from the model fit curve.

Data for prediction	Data for fit	Model	S.E. of the prediction
IRE-TREAT-Ctrl	IRE-TREAT-Fe IRE-SunTag-Ctrl	Flux (2.1.3)	6.1734
		Flux (2.1.2)	23.2938
		Flux (2.1.1)	14.6511
		Ribo. Nb. (2.2)	16.8179
SL-TREAT	IRE-TREAT-Fe SL-SunTag	Flux (2.1.3)	8.6444
		Flux (2.1.2)	3.2419
		Flux (2.1.1)	9.0909
		Ribo. Nb. (2.2)	10.92
NoSL-TREAT	IRE-TREAT-Fe NoSL-SunTag	Flux (2.1.3)	8.2453
		Flux (2.1.2)	4.8928
		Flux (2.1.1)	5.8548
		Ribo. Nb. (2.2)	7.0478
IRE-ShortORF-TREAT-Fe	IRE-TREAT-Fe IRE-SunTag-Fe	Flux (2.1.3)	7.8974
		Flux (2.1.2)	5.1230
		Flux (2.1.1)	9.6330
		Ribo. Nb. (2.2)	61.6324
IRE-ShortORF-TREAT-Ctrl	IRE-TREAT-Fe IRE-SunTag-Ctrl	Flux (2.1.3)	9.7746
		Flux (2.1.2)	37.8391
		Flux (2.1.1)	25.9392
		Ribo. Nb. (2.2)	61.5611
IRE-LongORF-TREAT-Fe	IRE-TREAT-Fe IRE-SunTag-Fe	Flux (2.1.3)	5.5203
		Flux (2.1.2)	7.3510
		Flux (2.1.1)	13.0370
		Ribo. Nb. (2.2)	16.1016
IRE-LongORF-TREAT-Ctrl	IRE-TREAT-Fe IRE-SunTag-Ctrl	Flux (2.1.3)	7.4522
		Flux (2.1.2)	29.5127
		Flux (2.1.1)	21.5657
		Ribo. Nb. (2.2)	13.0098
TPI-PTC160-Ctrl	TPI-PTC160-Fe IRE-SunTag-Fe	Flux-NMD	5.6271
Let7-IRE-TREAT-Fe	Let7-IRE-TREAT-Fe IRE-SunTag-Fe	Flux-miRNA	9.3868
miR21-IRE-TREAT-Fe	miR21-IRE-TREAT-Fe IRE-SunTag-Fe	Flux-miRNA	11.8539

Table 3: Prediction of the different models. Standard error (S.E.) of the prediction is the square root of the average squared distance that the observed values fall from the model prediction curve.

Data	Parameter	Best fit value	95% c.i.	S.E. of the fit
TPI-PTC160-Fe	Flux-NMD model			
	p_{NMD}	0.0348	$(0.022, 0.055)$	5.2587
Let7-IRE-TREAT-Ctrl	Flux-miRNA model			
	δ_{mi}	0.8307	$(0.56, 1.18)$	6.062
miR21-IRE-TREAT-Ctrl	Flux-miRNA model			
	δ_{mi}	0.1844	$(0.118, 0.242)$	7.4108

Table 4: Best fit parameter values for the NMD and miRNA models. All the rates are in $1/\text{hour}$. Standard error (S.E.) of the fit is the square root of the average squared distance that the observed values fall from the model fit curve.

7 Supplementary Figures

References

Peccoud, J and B Ycart (1995). "Markovian modelling of gene product synthesis". In: *Theoretical Population Biology*, pp. 1–13.

Xu, Heng et al. (2016). "Stochastic Kinetics of Nascent RNA". In: *Phys. Rev. Lett.* 117 (12), p. 128101.

Fu, Xiaoming et al. (2022). "Quantifying how post-transcriptional noise and gene copy number variation bias transcriptional parameter inference from mRNA distributions". In: *bioRxiv*. DOI: 10.1101/2021.11.09.467882.

Gupta, Ankit, Jan Mikelson, and Mustafa Khammash (2017). "A finite state projection algorithm for the stationary solution of the chemical master equation". In: *The Journal of Chemical Physics* 147.15, p. 154101.

Pawitan, Y. (2001). *In All Likelihood: Statistical Modelling and Inference Using Likelihood*. New York, New York: Oxford Science Publications, Clarendon Press, Oxford.

Gillespie, Daniel T. (1977). "Exact stochastic simulation of coupled chemical reactions". In: *The Journal of Physical Chemistry* 81.25, pp. 2340–2361. DOI: 10.1021/j100540a008.

Barrio, Manuel et al. (2006). "Oscillatory Regulation of Hes1: Discrete Stochastic Delay Modelling and Simulation". In: *PLOS Computational Biology* 2.9, pp. 1–14. DOI: 10.1371/journal.pcbi.0020117.

Burnham, K.P. and D.R. Anderson (2002). *Model selection and multimodel inference: a practical information-theoretic approach*. Springer Verlag.

Hoek, Tim A. et al. (2019). "Single-Molecule Imaging Uncovers Rules Governing Nonsense-Mediated mRNA Decay". In: *Molecular Cell* 75.2, 324–339.e11. ISSN: 1097-2765.

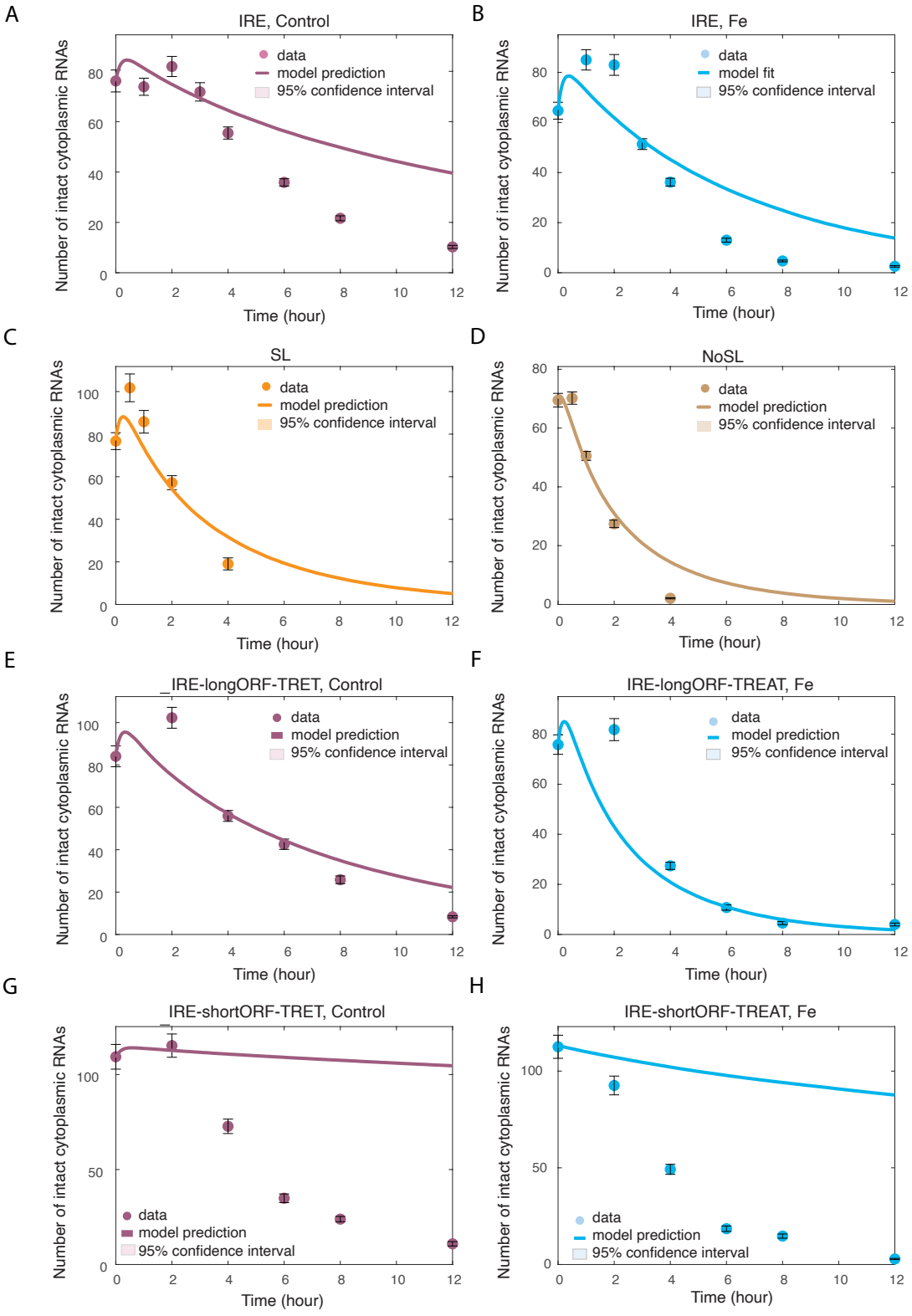

Figure 1: Ribosome flux degradation model with fixed probability to degrade after each initiation event. The dots represent experimental data. The solid lines represent the model fit or prediction, as indicated. Shaded area represents the 95% confidence interval of the parameter p_δ. (A) IRE-TREAT mRNAs in absence of the Fe; (B) IRE-TREAT mRNAs in presence of the Fe; (C) SL-TREAT mRNAs; (D) NoSL-TREAT mRNAs; (E) IRE-longORF-TREAT mRNAs in absence of Fe; (F) IRE-longORF-TREAT mRNAs in presence of Fe; (G) IRE-shortORF-TREAT mRNAs in absence of Fe; (H) IRE-shortORF-TREAT mRNAs in presence of Fe.

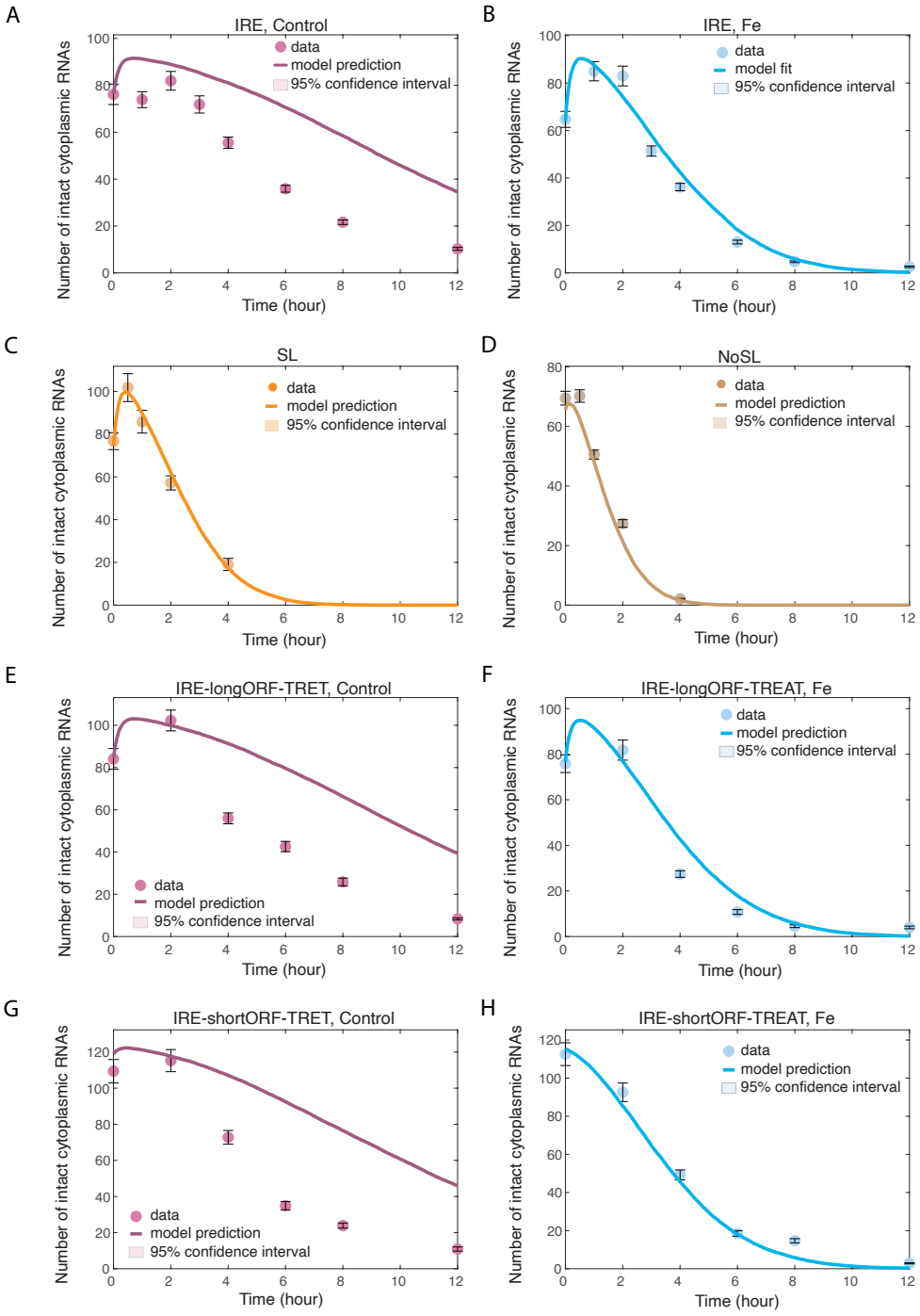

Figure 2: Ribosome flux degradation model with increasing probability to degrade after each initiation event. The dots represent experimental data. The solid lines represent the model fit or prediction, as indicated. Shaded area represents the 95% confidence interval of the parameter p_δ. (A) IRE-TREAT mRNAs in absence of the Fe; (B) IRE-TREAT mRNAs in presence of the Fe; (C) SL-TREAT mRNAs; (D) NoSL-TREAT mRNAs; (E) IRE-longORF-TREAT mRNAs in absence of Fe; (F) IRE-longORF-TREAT mRNAs in presence of Fe; (G) IRE-shortORF-TREAT mRNAs in absence of Fe; (H) IRE-shortORF-TREAT mRNAs in presence of Fe.

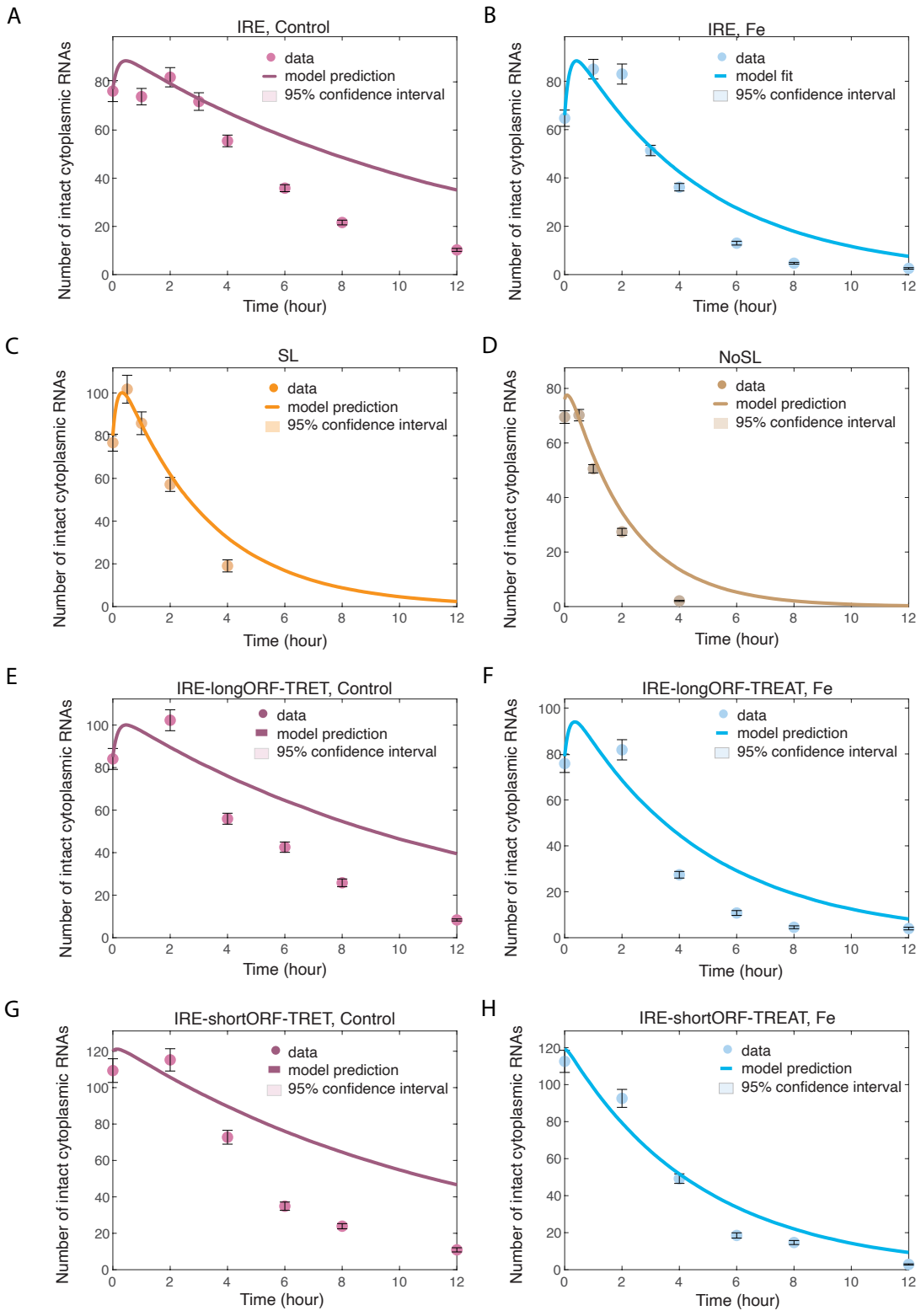

Figure 3: Ribosome number degradation model (degradation rate proportional to the number of ribosome on the template). The dots represent experimental data. The solid lines represent the model fit or prediction, as indicated. Shaded area represents the 95% confidence interval of the parameter p_δ. (A) IRE-TREAT mRNAs in absence of the Fe; (B) IRE-TREAT mRNAs in presence of the Fe; (C) SL-TREAT mRNAs; (D) NoSL-TREAT mRNAs; (E) IRE-longORF-TREAT mRNAs in absence of Fe; (F) IRE-longORF-TREAT mRNAs in presence of Fe; (G) IRE-shortORF-TREAT mRNAs in absence of Fe; (H) IRE-shortORF-TREAT mRNAs in presence of Fe.